



Aluminum Hydroxide Solubility in Sodium Hydroxide Solutions Containing Nitrite/Nitrate of Relevance to Hanford Tank Waste

September 2018

CH Delegard
CI Pearce
M Dembowski
MM Valenta-Snyder

II Leavy
SR Baum
MS Fountain

DISCLAIMER

This report was prepared as an account of work sponsored by an agency of the United States Government. Neither the United States Government nor any agency thereof, nor Battelle Memorial Institute, nor any of their employees, makes **any warranty, express or implied, or assumes any legal liability or responsibility for the accuracy, completeness, or usefulness of any information, apparatus, product, or process disclosed, or represents that its use would not infringe privately owned rights.** Reference herein to any specific commercial product, process, or service by trade name, trademark, manufacturer, or otherwise does not necessarily constitute or imply its endorsement, recommendation, or favoring by the United States Government or any agency thereof, or Battelle Memorial Institute. The views and opinions of authors expressed herein do not necessarily state or reflect those of the United States Government or any agency thereof.

PACIFIC NORTHWEST NATIONAL LABORATORY
operated by
BATTELLE
for the
UNITED STATES DEPARTMENT OF ENERGY
under Contract DE-AC05-76RL01830

Printed in the United States of America

Available to DOE and DOE contractors from the
Office of Scientific and Technical Information,
P.O. Box 62, Oak Ridge, TN 37831-0062;
ph: (865) 576-8401
fax: (865) 576-5728
email: reports@adonis.osti.gov

Available to the public from the National Technical Information Service
5301 Shawnee Rd., Alexandria, VA 22312
ph: (800) 553-NTIS (6847)
email: orders@ntis.gov <<http://www.ntis.gov/about/form.aspx>>
Online ordering: <http://www.ntis.gov>

Aluminum Hydroxide Solubility in Sodium Hydroxide Solutions Containing Nitrite/Nitrate of Relevance to Hanford Tank Waste

September 2018

CH Delegard¹
CI Pearce
M Dembowski
MM Valenta-Snyder

II Leavy
SR Baum
MS Fountain

Prepared for
the U.S. Department of Energy
under Contract DE-AC05-76RL01830

Pacific Northwest National Laboratory
Richland, Washington 99352

¹ TradeWind Services LLC

Abstract

The technical basis to support the One System River Protection Project Integrated Flowsheet assumption for diluting staged direct feed low-activity waste (DFLAW) from the Hanford waste tanks with raw river water must be assessed in light of the risk of aluminum hydroxide (gibbsite) precipitation prior to the subsequent transfer of tank contents into the low-activity waste pretreatment system (LAWPS) and/or the Tank Side Cesium Removal (TSCR) system from days to months after dilution. Aluminum solubility must be predicted as a function of the significant variables that influence gibbsite dissolution and precipitation. These variables include (i) other solution components that meaningfully affect the activity coefficient of either hydroxide or the aluminate ion, particularly nitrate and nitrite; and (ii) temperature. Based on a review of waste solubility data and the impact of dilution on solution stabilities with specific focus on aluminum hydroxide (Delegard et al. 2018), data gaps associated with the impact of these variables on the prediction of gibbsite solubility with temperature were identified. An experimental program to aid in the prediction of gibbsite solubility in NaOH solutions containing a range of sodium nitrate and sodium nitrite concentrations up to the solubility limit at a range of temperatures has been conducted. The results of these investigations are summarized in this report.

Executive Summary

The technical basis to support the One System River Protection Project Integrated Flowsheet assumption for diluting staged direct feed low-activity waste (DFLAW) from the Hanford waste tanks with raw river water must be assessed considering the risk of aluminum hydroxide (gibbsite) precipitation prior to the subsequent transfer of tank contents into the low-activity waste pretreatment system (LAWPS) and/or the Tank Side Cesium Removal (TSCR) system from days to months after dilution. Aluminum solubility must be predicted as a function of the significant variables that influence gibbsite dissolution and precipitation. These variables include (i) other solution components that meaningfully affect the activity coefficient of either hydroxide or the aluminate ion, particularly nitrate and nitrite; and (ii) temperature.

Based on a review of waste solubility data and the impact of dilution on solution stabilities with a specific focus on aluminum hydroxide (Delegard et al. 2018), data gaps associated with the impact of these variables on prediction of gibbsite solubility with temperature were identified. To address these gaps, experiments have been performed to study the impacts of sodium nitrate and sodium nitrite on gibbsite solubility as functions of sodium hydroxide concentration and temperature. Relative hydroxide and aluminum concentrations were chosen to be above, at, and below the 2:1 hydroxide:aluminum molar threshold observed for actual tank waste solutions. The solubility experiments were conducted with well-characterized finely crystalline hexagonal (~0.3 μm across, ~0.03 μm thick) synthetic aluminum hydroxide (gibbsite) particles that are broadly representative of the solubility-controlling finely crystalline gibbsite particles present in actual tank waste. Using this synthetic gibbsite, the time to attainment of equilibrium aluminum solution concentrations was established (i) through dissolution of gibbsite at a range of temperatures (bottom-up approach) and (ii) through the precipitation of aluminum-bearing solids at 45 °C from a solution first saturated with gibbsite at 80 °C (top-down approach). The results of these experiments are summarized in this report.

The presence of added NaNO_3 , NaNO_2 , and NaNO_3 - NaNO_2 in combination in every case enhanced the aluminum solution concentration (gibbsite solubility) above that expected from the Misra (1970) Equation at the same respective NaOH concentrations but in the absence of added salt. The solubility enhancements observed at 27 °C and 45 °C for NaNO_3 and NaNO_2 were roughly equivalent (though with nitrite showing a slightly greater effect than nitrate), and markedly lower than what was found at 80 °C. However, mole-for-mole, the enhancement effect at 80 °C for NaNO_2 was much greater than that found for NaNO_3 .

The attainment of steady dissolved aluminum concentrations was fairly rapid (days) in the presence of the gibbsite solids (bottom-up), but precipitation from oversaturation (top-down) was not complete even after seven weeks or more at 45 °C and only was completed upon addition of gibbsite seed crystals.

Characterization of the solid phases by X-ray diffraction (XRD) and scanning electron microscopy (SEM), before and after aging in the different saturated solutions, revealed the solid phase remained gibbsite, but that recrystallization occurred to form larger crystallites.

Further testing beyond the results summarized in this report will be necessary to establish the key factors in gibbsite precipitation delay and rate. Among these avenues of testing are the following:

- Determine the concentration of sodium nitrite in solution as a function of temperature, as this affects the activity coefficient of the hydroxide and the aluminate ion. There are very few studies of the NaNO_2 - NaOH - H_2O system in the literature. The proposed task will close the identified data gap associated with the NaNO_2 - NaOH - H_2O system at temperatures greater than 25 °C.

- Establishment of the importance of dawsonite, $\text{NaAlCO}_3(\text{OH})_2$, and carbonate on $\text{Al}(\text{OH})_3$ dissolution and precipitation.
- Understanding the effect of gibbsite seed crystals as a means of inducing precipitation and mitigating the effects of unanticipated solids carryover into the LAWPS caused by delayed aluminum precipitation (e.g., fouling the LAWPS ion exchange operations and transfer line deposition).
- Extension of the experimental timescale to encompass anticipated storage intervals for diluted DFLAW (i.e., one to nine months) to understand $\text{Al}(\text{OH})_3$ precipitation kinetics.
- Definition of sodium counterion concentrations needed to stabilize polymeric aluminum solution species and limit precipitation.

Ultimately, this additional work would provide key information about (1) the mechanisms by which gibbsite becomes supersaturated; (2) $\text{Al}(\text{OH})_3$ precipitation kinetics, including induction times to precipitation; and (3) potential blending strategies to minimize $\text{Al}(\text{OH})_3$ precipitation or seeding strategies to manage precipitation.

Acknowledgments

This work was completed in support of the One System River Protection Project Integrated Flowsheet. Funding for this project came from Washington River Protection Solutions. The authors wish to acknowledge Jacob Reynolds (Washington River Protection Solutions) for programmatic guidance, direction, and support. The authors acknowledge Odeta Qafoku for measuring the surface area of the gibbsite. We are also grateful to our technical reviewers—Reid Peterson, Keith Geiszler, Courtney Bottenus, and Arich Fuher—for their meticulous examinations of the various spreadsheets and calculations and Bill Dey for his overall quality review. Finally, we thank Heather Culley for her technical editing.

Acronyms and Abbreviations

BET	Brunauer-Emmett-Teller
CCB	continuing calibration blank
CCV	continuing calibration verification
DFLAW	direct feed low-activity waste
DIW	deionized water
EFRC	Energy Frontier Research Center
ESL	Environmental Science Laboratory
FMP	flowsheet maturation plan
FWHM	full width half maximum
FY	fiscal year (October 1 through September 30; e.g., FY 2018 ends on September 30, 2018)
HASQARD	Hanford Analytical Services Quality Assurance Requirements Documents
IC	ion chromatography
ICDD	International Centre for Diffraction Data
ICP	inductively coupled plasma
ICP-AES	inductively coupled plasma-atomic emission spectroscopy
ICP-OES	inductively coupled plasma-optical emission spectrometer/spectroscopy
ICV	initial calibration verification
IDREAM	Interfacial Dynamics in Radioactive Environments and Materials
LAWPS	low-activity waste pretreatment system
MDL	method detection limit
NIST	National Institute of Standards and Technology
NMR	nuclear magnetic resonance
NQA	nuclear quality assurance
PNNL	Pacific Northwest National Laboratory
QA	quality assurance
QC	quality control
R&D	research and development
RSD	relative standard deviation
SEM	scanning electron microscopy
TSCR	Tank Side Cesium Removal
TWINS	Tank Waste Information Network System
WRPS	Washington River Protection Solutions
WTP	Hanford Tank Waste Treatment and Immobilization Plant
WWFTP	WRPS Waste Form Testing Program
XRD	X-ray diffraction

Contents

Abstract.....	iii
Executive Summary.....	iv
Acknowledgments.....	vi
Acronyms and Abbreviations	vii
1.0 Introduction and Background.....	1.1
2.0 Technical Approach and Scope.....	2.1
2.1 Quality Assurance.....	2.1
2.2 Gibbsite Synthesis and Characterization.....	2.1
2.3 Gibbsite Solubility Tests.....	2.2
2.4 Chemical Analysis.....	2.4
2.5 Solid Phase Characterization.....	2.5
3.0 Results and Discussion.....	3.1
3.1 Gibbsite Qualification	3.1
3.1.1 X-ray Diffraction (XRD)	3.1
3.1.2 Scanning Electron Microscopy and Surface Area	3.1
3.2 Gibbsite Solubility Tests.....	3.3
3.2.1 Attaining Steady-State Aluminum Concentration from Undersaturation.....	3.3
3.2.2 Attaining Steady-State Aluminum Concentration from Oversaturation at 45 °C.....	3.7
3.2.3 Measured Gibbsite Solubility in Current Tests versus Misra (1970) Predicted Solubility	3.10
3.2.4 Measured Gibbsite Solubility in Current Tests in Molality Units	3.12
3.2.5 Gibbsite Solubility in NaOH-NaAl(OH) ₄ -NaNO ₃ Solutions.....	3.14
3.2.6 Gibbsite Solubility in NaOH-NaAl(OH) ₄ -NaNO ₃ -NaNO ₂ Solutions.....	3.18
3.2.7 Gibbsite Solubility in NaOH-NaAl(OH) ₄ -NaNO ₂ Solutions.....	3.18
3.3 Solid Phase Characterization after Dissolution Tests.....	3.19
3.3.1 Effect of Dissolution from Undersaturation on Gibbsite Mineralogy and Particle Size.....	3.19
3.3.2 Effect of Dissolution from Undersaturation and Oversaturation on Gibbsite at 45 ± 2 °C.....	3.20
4.0 Summary and Conclusions	4.1
4.1 Proposed Task 3 Work Scope	4.2
4.2 Recommendations for Follow-On Work.....	4.3
5.0 References	5.1
Appendix A – Experimental Set-Up Pictures	A.1
Appendix B – Starting Solution Conditions for Sodium Hydroxide Containing Sodium Nitrite/Nitrate..	B.1
Appendix C – Gibbsite Solubility Tests at 80 °C	C.1
Appendix D – Gibbsite Solubility Data.....	D.1
Appendix E – Post-Test XRD.....	E.1

Figures

1	XRD of Gibbsite Nanoplate Starting Material.....	3.1
2	SEM of Gibbsite Solids Used in the Solubility Tests	3.2
3	Gibbsite Solubility in 27 °C, 1 m NaOH Solutions with Varying [NaNO ₃] and [NaNO ₂].....	3.5
4	Gibbsite Solubility in 45 °C Tests with Varying [NaNO ₃] and [NaNO ₂].....	3.5
5	Gibbsite Solubility in 80 °C, 2 m NaOH Solutions with Varying [NaNO ₃] and [NaNO ₂].....	3.6
6	Gibbsite Solubility in 6 m NaOH Solutions at Varying Temperatures.....	3.6
7	Aluminum Concentrations versus Time for Tests T5 and T13.....	3.8
8	Aluminum Concentrations versus Time for Tests T6 and T14.....	3.8
9	Aluminum Concentrations versus Time for Tests T7 and T15.....	3.9
10	Aluminum Concentrations versus Time for Tests T8 and T16.....	3.9
11	Measured Gibbsite Solubility in Current Tests versus Misra Equation Predicted Solubility in NaOH Solutions as Functions of NaOH Concentration and Temperature	3.11
12	Measured Gibbsite Solubility in 27 °C Tests with ~ 1 m NaOH with Hydroxide and Aluminum Concentrations Expressed in Molality Versus Predicted Solubility in NaNO ₃ /NaNO ₂ -free NaOH/NaAl(OH) ₄ Solutions as Functions of NaOH Concentration	3.13
13	Measured Gibbsite Solubility in 27 °C Tests with Hydroxide and Aluminum Concentrations Expressed in Molality Versus Predicted Solubility in NaNO ₃ /NaNO ₂ -free NaOH/NaAl(OH) ₄ Solutions as Functions of NaOH Concentration.....	3.14
14	Gibbsite Solubility in the Presence of NaNO ₃	3.16
15	Gibbsite Solubility in the Presence of NaNO ₃ at Near Room Temperature in Tests from Both Undersaturation and Oversaturation	3.17
16	XRD showing changes to the gibbsite mineralogy and particle size at 27 ± 2 °C, 45 ± 2 °C, and 80 ± 2 °C after exposure to NaOH solution	3.20
17	SEM Showing Changes to the Size and Morphology of Gibbsite Solid Phase at 45 ± 2 °C after Exposure to NaOH/NaNO ₂ Solution; NaOH/NaNO ₃ Solution; NaOH/NaNO ₃ /NaNO ₂ Solution; and NaOH Solution.....	3.21
18	XRD Showing Changes to the Gibbsite Solid Phase and Crystallinity at 45 ± 2 °C after Exposure to: NaOH/NaNO ₂ Solution; NaOH/NaNO ₃ Solution; NaOH/NaNO ₃ /NaNO ₂ Solution; and NaOH Solution.....	3.22

Tables

1	Target Solution Conditions for Gibbsite Solubility Tests at a Range of Temperatures.....	2.2
2	Calculated Test Conditions based on Target Concentrations for Gibbsite Solubility Tests at a Range of Temperatures	2.3
3	Experimental Conditions, Based on Masses of Materials Added, and Plateau Aluminum Concentration Findings in Molality and Molarity	3.3
4	Experimental Conditions for Tests at 45 °C Approaching Steady State from Undersaturation and Oversaturation	3.7

1.0 Introduction and Background

Pacific Northwest National Laboratory (PNNL) provides Washington River Protection Solutions (WRPS) baseline technical support to the Mission Integration team to identify and close flowsheet model and operations gaps and realize opportunities to reduce the waste treatment mission cost, schedule, and technical risk. These flowsheet gaps and opportunities are documented in RPP-PLAN-58003, One System River Protection Project Integrated Flowsheet Maturation Plan, and solution approaches are proposed and declared in associated flowsheet maturation plans (FMPs) contained in the appendices of RPP-PLAN-58003. This report fulfills Task 2 of the flowsheet maturation plan, FMP-DFLAW-25, “Aluminum Hydroxide Solubility in Sodium Hydroxide Solutions Containing Nitrite/Nitrate.”

The current integrated flowsheet model, described and documented in One System River Protection Project Integrated Flowsheet (Anderson et al. 2017), assumes raw filtered river water is used at all times to dilute the direct feed low-activity waste (DFLAW) staged feed tank prior to the subsequent transfer into the low-activity waste pretreatment system (LAWPS) from days to months after dilution. However, no technical basis has been identified and documented to support this assumption while protecting against aluminum hydroxide precipitation. A review of waste solubility data and the impact of up to nine months’ time following dilution with water, with specific focus on aluminum hydroxide (Task 1 of FMP-DFLAW-25 [Reynolds et al. 2017]), identified gaps in predicting aluminum hydroxide solubility with dilution and temperature (Delegard et al. 2018). The purpose of this research program is to close gaps and obtain solubility relationships between aluminum hydroxide and other ions to more accurately model the solubility of gibbsite (one of the mineral forms of aluminum hydroxide) and the rates of its dissolution and crystallization.

In fiscal year (FY) 2018, WRPS has contracted with PNNL to close the identified data gaps so that aluminum solubility can be predicted as a function of the significant variables that influence gibbsite dissolution and precipitation. These variables are (i) the presence of nitrate and nitrite as solution components that meaningfully affect the activity coefficient of hydroxide and/or the aluminate ion, and (ii) temperature. Nitrate and nitrite are particularly important in Hanford Site tank wastes by their potential impacts on gibbsite solubility because of their ubiquity and relatively high concentrations compared with other tank waste salts. This work supports the One System River Protection Project Mission Integration team to identify and close flowsheet model and operations gaps and realize opportunities to reduce the waste treatment mission cost, schedule, and technical risk. These flowsheet gaps and opportunities are documented in the One System River Protection Project Integrated Flowsheet Maturation Plan (Reynolds et al. 2017) and solution approaches are proposed and declared in associated FMPs contained in its appendices. The major deliverable of this task is a final report covering results, discussions, conclusions, and recommendations for future tests.

2.0 Technical Approach and Scope

2.1 Quality Assurance

This work was conducted with funding from WRPS under Project 71351, Contract 36437-239, with the title “Tank Waste Disposition Integrated Flowsheet Support.”

All research and development (R&D) work at PNNL is performed in accordance with PNNL’s Laboratory-Level Quality Management Program, which is based on a graded application of NQA-1-2000, *Quality Assurance Requirements for Nuclear Facility Applications*, to R&D activities. To ensure that all client quality assurance (QA) expectations were addressed, the QA controls of the WRPS Waste Form Testing Program (WWFTP) QA program were also implemented for this work. The WWFTP QA program implements the requirements of NQA-1-2008, *Quality Assurance Requirements for Nuclear Facility Applications*, and NQA-1a-2009, *Addenda to ASME NQA-1-2008*, and consists of the WWFTP Quality Assurance Plan (QA-WWFTP-001) and associated procedures that provide detailed instructions for implementing NQA-1 requirements for R&D work.

Preparation of this report was assigned the technology level “Applied Research,” and was planned, performed, documented, and reported in accordance with procedure QA-NSLW-1101, *Scientific Investigation for Applied Research*. All staff members contributing to the new experimental work and findings received appropriate technical and QA training prior to performing quality-affecting work. Note that the QA controls described above for others’ findings as given in published technical literature apply only to the compilation, review, analysis, and reporting of the information from the source documents cited in this report; the QA pedigree of the information in each source document is determined by the controls implemented by its author(s) and originating organization.

2.2 Gibbsite Synthesis and Characterization

Gibbsite synthesis and Brunauer-Emmett-Teller (BET) analysis was conducted as part of PNNL’s Interfacial Dynamics in Radioactive Environments and Materials (IDREAM) Energy Frontier Research Center (EFRC). Briefly, gibbsite was synthesized using a hydrothermal method as described in Zhang et al. (2017) according to the following general method. First, aluminum nitrate nonahydrate ($\text{Al}(\text{NO}_3)_3 \cdot 9\text{H}_2\text{O}$) was dissolved in deionized water (DIW) with stirring, forming a homogeneous solution with a concentration of 0.25 M at room temperature. A sodium hydroxide (NaOH) solution was added to the aqueous solution to adjust the pH to ~5.0. The resulting gel-like precipitates were stirred at room temperature for one hour and were subsequently collected by centrifugation. The gel was re-dispersed in 18 M Ω -cm water and centrifuged three times to remove any residual sodium and nitrate (Na^+ and NO_3^-) ions. The washed gel was re-dispersed in 18 M Ω -cm water, transferred to a Teflon autoclave, sealed into a Parr bomb, and heated in an electric oven equipped with a rotating element (80 °C, ca. 10 rpm) for 96 hours. The product was recovered by centrifugation, washed with DIW, and dried overnight. Because of their small hexagonal particle size and aspect (~0.3 μm width, ~0.03 μm thickness), we called these synthetic gibbsite particles “nanoplates”.

The specific surface area of the gibbsite product was measured with an Accelerated Surface Area and Porosity System ASAP 2020, from Micromeritics. The sample was degassed at 75 °C for nine hours, with a temperature ramp of 5 °C/min. A Si-Alumina standard (Micromeritics) with a known surface area of $214 \pm 6 \text{ m}^2/\text{g}$ was analyzed immediately after the sample. The measured surface area of the standard was $212 \text{ m}^2/\text{g}$, which is within the accepted standard deviation range for the instrument.

To qualify the gibbsite for use in the solubility tests, its mineralogy was confirmed using X-ray diffraction (XRD). The XRD instrument used for this analysis was a Rigaku Miniflex II Bragg-Brentano diffractometer using Cu-K α radiation ($\lambda = 1.5406 \text{ \AA}$) and a graphite post-diffraction monochromator. Powders were loaded into zero-background holders with a rutile (TiO $_2$) standard added to each sample as the internal standard. Data was taken from 5 to 65 degrees 2-theta with a step size of 0.02 degree 2-theta and a counting time between 2 and 19 seconds per step. Phases were identified with the JadeTM computer software (Materials Data Incorporated) search match routines with comparison to the International Centre for Diffraction Data (ICDD) database, which includes the Inorganic Crystal Structure Database. The morphology of the gibbsite was characterized by scanning electron microscopy (SEM) using a Helios NanoLab 600i SEM (FEI, Hillsboro, OR). Powder samples were sputter coated with a thin layer of carbon to ensure good conductivity and imaging. The SEM images were used to confirm morphology consistency.

2.3 Gibbsite Solubility Tests

The gibbsite solubility tests were set up in the matrix shown in Table 1.

Table 1. Target Solution Conditions (Concentrations of Sodium, Hydroxide, Nitrite, and Nitrate in molal) for Gibbsite Solubility Tests at a Range of Temperatures

Test	Na (m)	OH ⁻ _{init} (m)	NO $_2^-$ (m)	NO $_3^-$ (m)	Temperature (°C)
T0	1.0	1.0	0.0	0.0	27
T1	8.0	1.0	7.0	0.0	27
T2	6.0	1.0	0.0	5.0	27
T3	11.0	1.0	5.0	5.0	27
T4	6.0	6.0	0.0	0.0	27
T5	10.0	1.0	9.0	0.0	45
T6	7.0	1.0	0.0	6.0	45
T7	14.0	4.0	5.0	5.0	45
T8	6.0	6.0	0.0	0.0	45
T9	12.0	2.0	10.0	0.0	80
T10	10.0	2.0	0.0	8.0	80
T11	18.0	2.0	8.0	8.0	80
T12	6.0	6.0	0.0	0.0	80
T13	10.0	1.0	9.0	0.0	80 cooled to 45
T14	7.0	1.0	0.0	6.0	80 cooled to 45
T15	14.0	4.0	5.0	5.0	80 cooled to 45
T16	6.0	6.0	0.0	0.0	80 cooled to 45

The tests build on experiments described in Barney (1976), Herting et al. (1986), Bénézech et al. (2016), Reynolds et al. (2016), and the associated lab report McCoskey et al. (2015). The temperatures were selected to range from laboratory temperature (~27 °C), which is somewhat higher than the lowest tank waste temperature, up to 80 °C, so as to remain below the temperature threshold for the hydrothermal transformation of gibbsite to boehmite but include temperatures anticipated in gibbsite and boehmite dissolution processing from tank wastes. The hydroxide concentrations were selected to range from those having appreciable aluminate equilibrium concentrations (i.e., down to 1 m NaOH) to the greatest found in tank waste (6 m NaOH). The NaNO $_3$ and NaNO $_2$ concentrations were selected to be, where used, as high as possible without exceeding their respective solubilities as described in Reynolds and Herting (1984), and thus vary from one salt to the other and with temperature. The evidence for Hanford tank wastes being saturated in NaNO $_3$ is abundant, but few instances of NaNO $_2$ solids being found in tank

waste are known (Herting et al. 2015). Effort was also made to ensure that some instances of total sodium concentration were near the 13–15 M maximum found in actual tank wastes. To minimize uptake of atmospheric carbon dioxide in the alkaline test solutions and thus eliminate the confounding influence of sodium carbonate, all tests took place in an argon-purged glovebox.

The solubility of gibbsite in solutions of $\text{NaAl(OH)}_4\text{-NaOH}$ at a variety of temperatures can be modeled by the Misra solubility equation (Misra 1970; Delegard et al. 2018). The Misra Equation [Equation (1)] is valid from 25 to 100 °C and for caustic concentrations of ~1 to 7.4 M total sodium. Equation (1) (henceforth the Misra Equation) was used in this study to predict Al concentrations as a function of the test conditions in Table 2.

$$\ln ([\text{Al}], \text{M}) = 5.7128 - 2486.7/(\text{T}, \text{K}) + 33.702([\text{NaOH}], \text{M})/(\text{T}, \text{K}) + \ln ([\text{NaOH}], \text{M}) \quad (1)$$

where NaOH represents total alkalinity present both as free NaOH and combined with aluminum as NaAl(OH)_4 .

Table 2. Calculated Test Conditions (Concentrations of Sodium Hydroxide, Sodium Nitrite, Sodium Nitrate, and Sodium Aluminate in Moles and Amount of Gibbsite Added) based on Target Concentrations (Table 1) for Gibbsite Solubility Tests at a Range of Temperatures

Test	Temp (°C)	Density ^a (g/mL)	Starting NaOH (M)	NaNO ₃ (M)	NaNO ₂ (M)	Final NaOH ^b (M)	NaAl(OH) ₄ ^b (M)	Al(OH) ₃ ^c (g)
T0	27	1.036	1.00	0.00	0.00	0.912	0.085	0.2
T1	27	1.274	0.84	0.00	5.86	0.767	0.070	0.2
T2	27	1.258	0.86	4.29	0.00	0.787	0.072	0.2
T3	27	1.391	0.77	3.84	3.84	0.705	0.064	0.2
T4	27	1.232	5.96	0.00	0.00	5.074	0.885	1.5
T5	45	1.328	0.80	0.00	7.20	0.694	0.106	0.3
T6	45	1.295	0.84	5.01	0.00	0.725	0.111	0.3
T7	45	1.481	3.07	3.84	3.84	2.553	0.517	1.6
T8	45	1.232	5.96	0.00	0.00	4.598	1.364	2.6
T9	80	1.385	1.56	0.00	7.82	1.085	0.480	1.3
T10	80	1.395	1.59	6.34	0.00	1.099	0.487	1.3
T11	80	1.562	1.35	5.40	5.40	0.945	0.406	1.5
T12	80	1.233	5.97	0.00	0.00	3.182	2.784	5.3
T13	45	1.328	0.80	0.00	7.20	0.694	0.106	0.3
T14	45	1.295	0.84	5.01	0.00	0.725	0.111	0.3
T15	45	1.481	3.07	3.84	3.84	2.553	0.517	1.6
T16	45	1.232	5.96	0.00	0.00	4.598	1.364	3.4

^a Calculated per Orme (2003)

^b Calculated per the Misra Equation; i.e., Equation (1)

^c Values are actual targets providing excess Al(OH)_3 which were not less than 1.5-times the estimated requirements based on Misra Equation predictions for gibbsite solubility for 13 mL of NaNO_3 - and NaNO_2 -free NaOH/NaAl(OH)_4 solution

Starting solutions of sodium hydroxide (1, 2, 4, and 6 m) were prepared at the required temperature, and the required amount of sodium nitrite and/or sodium nitrate for each test was added. For example, according to Table 1, test T1 contained 1.0 m NaOH (0.84 M, Table 2, initial concentration) and 7.0 m (5.86 M) NaNO_2 at 27 °C. Aliquots of these starting solutions (13 mL) were added to (i) 15 mL Teflon tubes for tests conducted at 27 °C and 45 °C and (ii) 50 mL Teflon tubes for tests conducted at 80 °C to

allow space for solution expansion upon heating. Three different reaction vessels were prepared from the same starting solution for each test condition (e.g., T1-1, T1-2, and T1-3) and excess gibbsite nanoplate solid was added to each of the triplicates. Reaction vessels were sealed with threaded caps and the cap/tube outer joints wrapped with Teflon tape to limit evaporative water loss. The test vessels then were agitated in a thermostatted condition. Temperature control at 27 ± 2 °C was maintained for tests T0 through T4 in a thermostatted controlled atmosphere (argon) glovebox. Reaction vessels at this temperature were agitated using a rocking platform (Figure A.1). The tests at higher temperature (45 °C and 80 °C) were maintained in the argon-purged glovebox and heated in aluminum heat blocks on hot plates (Figure A.2). For each temperature, all tests and triplicates were run in the same heater block at the same time. Agitation was accomplished by magnetic stirrers at 600 ± 100 rpm. The magnetic stirrers were tapered for conical bottom tubes, and the hot plates had four individual stir plates, one for each heat block. In addition, all tubes were inspected and manually agitated twice-weekly to ensure adequate stirring. It is noted that in similar prior experiments, stir speed was found to have no noticeable effect on the rate of achieving steady Al concentrations (Bénézeth et al. 2016). The temperature in the aluminum blocks was regulated to ± 2 °C and checked regularly with a NIST-traceable thermometer. Actual temperatures were measured during each sampling.

In tests numbered T0 through T12 (Table 1), equilibrium was approached from below saturation (bottom-up), and sufficient gibbsite was added to exceed solubility. To ensure that sufficient gibbsite was added to the tests, an amount that was not less than 1.5 times the solubility predicted by Equation (1) was added (Table 2). In tests numbered T13 through T16 (Table 1), equilibrium was approached from oversaturation (top-down) by heating to 80 °C overnight, then cooling to 45 °C. Gibbsite was added at concentrations below expected solubility at 80 °C but above solubility at 45 °C. After 49 to 76 days at 45 °C, and with evidence of gibbsite precipitation for some tests as indicated by downward trending in aluminum concentration and the appearance of solids, seed crystals of the gibbsite starting material (0.4 g) were added to promote $\text{Al}(\text{OH})_3$ precipitation.

Aliquots (100 μL) were collected from the reaction vessels at temperature (over the test period of up to 146 days) using a pipette. Aliquots were filtered using 13-mm diameter 0.2- μm pore size PVDF (polyvinylidene difluoride) syringe filters to remove the solids. This filter medium is chemically resistant to the strongly alkaline test solutions. The weight of a known volume of filtered sample at test temperature was used to determine the density.

According to Bénézeth et al. (2016), samples taken as a function of time should reach constant Al concentration in less than 20 days, but sampling was continued until Al concentrations of three consecutive samples formed a horizontal asymptote as a function of time within experimental error. As discussed in Section 3.2.1, except for the tests conducted from oversaturation, aluminum concentrations attained near-equilibrium values within days. However, the contacts were continued for extended times to guarantee attainment of steady state.

2.4 Chemical Analysis

Solution analyses were performed in the Environmental Science Laboratory (ESL) of PNNL. Aluminum was analyzed quantitatively using a PerkinElmer Optima 8300 dual view inductively coupled plasma-optical emission spectrometer (ICP-OES) and a PerkinElmer S-10 auto-sampler interface. Aluminum was analyzed at a wavelengths of 396.153 nm (axial). The instrument was calibrated using standards made by the High-Purity Standards Corporation to generate calibration curves. The range of the calibration curves was 50 ppb to 50 ppm. This calibration was verified immediately with an initial calibration verification (ICV) and during sample analysis with a continuing calibration verification (CCV), which was run every ten samples at a minimum as per Hanford Analytical Services Quality Assurance Requirements

Documents (HASQARD, DOE/RL-96-68) requirements. Continuing calibration blanks (CCB) were also analyzed after each calibration verification to ensure background signals and potential carryover effects were not a factor. The calibration was independently verified using standards made by Inorganic Ventures. A 1 ppm lutetium, scandium, and yttrium solution was added as an online internal standard to all samples, standards, and blanks to demonstrate the stability of the instrument and sample introduction system. A method detection limit (MDL) of 16.47 ppb was established for Al by running the lowest calibration standard (50 ppb) six consecutive times and multiplying the standard deviation of those six replicates by 3.143 (student t-test value) to establish an instrument detection limit and then multiplying that number by five to get the MDL. This process was repeated three times on non-consecutive days and averaged to establish a working MDL in ppb. All samples and standards were diluted with 2% Fisher Scientific Optima trace metal grade nitric acid and DIW with resistivity no lower than 18.0 MΩ-cm.

Quantitative dilutions of the starting solution and final solution were analyzed quantitatively for NO₂⁻ and NO₃⁻ using either a Dionex Reagent Free Ion Chromatography System 5000 (RFICS-5000) with an AS-AP auto-sampler or a Dionex Reagent Free Ion Chromatography System 2000 (RFICS-2000) with an AS-1 auto-sampler. Both instruments were calibrated using a multi-component anion solution made by Inorganic Ventures. The calibrated range was 0.1 ppm to 7.5 ppm. The calibration was verified immediately with an ICV standard and during sample analysis with a CCV standard run every ten samples at a minimum. A CCB was analyzed after each CCV to ensure background signals and potential carryover effects were not a factor. The CCV standard was prepared from a multi-component anion solution made by SPEX CertiPrep.

Alkalinity of the final solutions was measured through titration, using a Metrohm 888 Titrando Titrator controlled by a personal computer running Tiamo 2.4 software, with 0.02 N sulfuric acid (H₂SO₄) to a phenolphthalein endpoint for total alkalinity (hydroxide plus aluminate).

All calibration verification values must be within ±10% of the target concentrations to comply with the QA/QC (quality control) requirements as defined in the HASQARD.

2.5 Solid Phase Characterization

To determine the effect of the solution test conditions on the gibbsite solid phase, selected samples were analyzed by XRD and SEM. The solids were vacuum filtered and washed with 200 proof ethanol to remove excess sodium salts, and dried at 40 °C for 24 hours. The XRD instrument used for this analysis was a Phillips diffractometer using CuKα radiation ($\lambda = 1.5406 \text{ \AA}$) and a graphite post-diffraction monochromator. Powders were loaded into zero-background holders and data were taken from 10 to 80 degrees 2-theta. Phases were identified with the JADE search match routines with comparison to the ICDD database, which includes the Inorganic Crystal Structure Database. Crystallite size was estimated from the Scherrer equation:

$$\tau = \frac{K\lambda}{\beta \cos\theta} \quad (2)$$

where τ is the mean size of the ordered (crystalline) domains, K is a shape factor ($K = 0.9$), λ is the X-ray wavelength, β is the line broadening at half the maximum intensity (full width half maximum—FWHM), and θ is the Bragg angle. Line broadening was measured with respect to that of synthetic silicon (ICDD ID: 04-001-7247). The morphology of the gibbsite after the conclusion of the experiment was characterized by SEM using a Helios NanoLab 600i SEM (FEI, Hillsboro, OR). Powder samples were mounted on a carbon tape and sputter coated with a thin layer of carbon (~15 nm) to ensure good conductivity and imaging.

3.0 Results and Discussion

3.1 Gibbsite Qualification

3.1.1 X-ray Diffraction (XRD)

XRD patterns as a function of 2θ based on $\text{CuK}\alpha$ radiation ($\lambda=1.5406 \text{ \AA}$) were measured to qualify the synthesized gibbsite starting material for use in the solubility tests. The calculated and observed background-subtracted XRD patterns for the starting material are shown in Figure 1, including the rutile internal standard. Gibbsite (ICDD ID: 04-011-1369) was the only crystalline solid phase identified by XRD. The relative broadness of the gibbsite peaks—for example, the basal plane thickness peak at $\sim 18.2^\circ$ 2-theta —indicates a small (24 nm) crystallite size and is consistent with the 29 nm thickness estimated from the SEM images (Section 3.1.2).

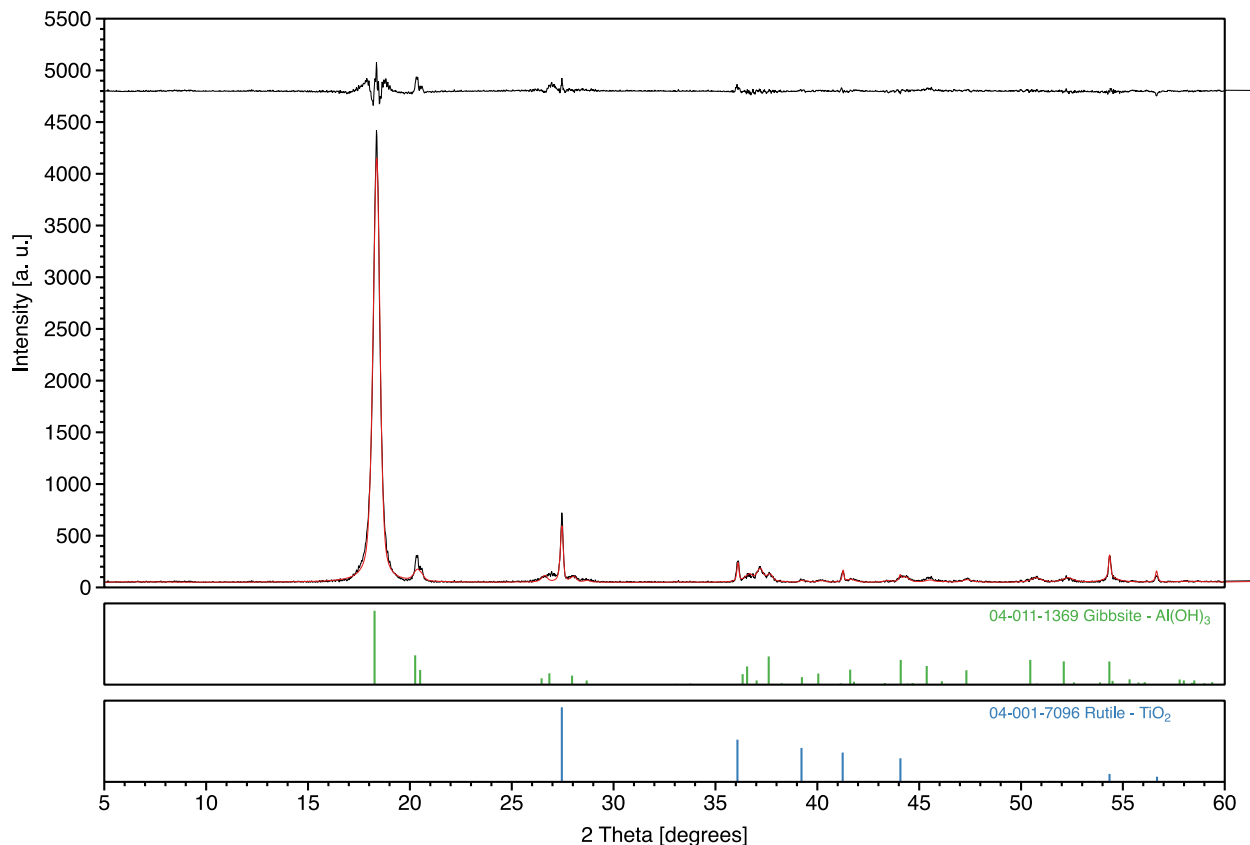


Figure 1. XRD of Gibbsite Nanoplate Starting Material

3.1.2 Scanning Electron Microscopy and Surface Area

The size and shape of gibbsite crystals are of importance in understanding Hanford tank waste chemistry. Studies summarized by Herting et al. (2015) show that gibbsite crystals present in Hanford tank wastes generally are small—beginning at 1–10 μm and ranging to hundreds of μm across—and have a pseudo-hexagonal habit. These dimensions, which were determined through a combination of optical microscopy and SEM, likely are biased toward higher sizes due to the difficulty of viewing smaller

particles by these techniques in this difficult matrix. In prior gibbsite solubility studies, Almatix Hydrated Alumina C333 gibbsite, with a particle size of $4.05\ \mu\text{m}$ and BET specific surface area of $4.83\ \text{m}^2/\text{g}$, was recommended as a simulant to mimic the particle size of actual waste gibbsite as determined by their respective SEM images (Figure 3.1 in Russell et al. 2009). However, the gibbsite particles visible by SEM in the actual waste likely are greater in size than the invisible smaller gibbsite particles that are solubility-controlling.

For the present work, highly uniform euhedral hexagonal gibbsite nanoplates synthesized using the methods described in Zhang et al. (2017) were used. SEM was used to characterize the size and morphological consistency of the synthesized gibbsite starting material (Figure 2). A statistical analysis of particle size from SEM data collected on gibbsite particles produced by this method indicated that the particle width and average thickness are $332 \pm 73\ \text{nm}$ and $29 \pm 7\ \text{nm}$, respectively. These sub-micron ($\sim 0.3\ \mu\text{m}$) particles are somewhat smaller than the $\sim 1\ \mu\text{m}$ lower threshold of that observed by scanning electron and optical microscopies in tank waste solids (Herting et al. 2015). The BET specific surface area of gibbsite starting material was $32.5\ \text{m}^2/\text{g}$. Overall, the small particle size and high surface area of the gibbsite nanoplates used in this work enhanced dissolution kinetics so that equilibrium could be reached within the timescale of the tests. This small particle size also more closely mimics the extant solubility-controlling solid phase conditions in incipient gibbsite crystallization and dissolution in actual tank wastes.

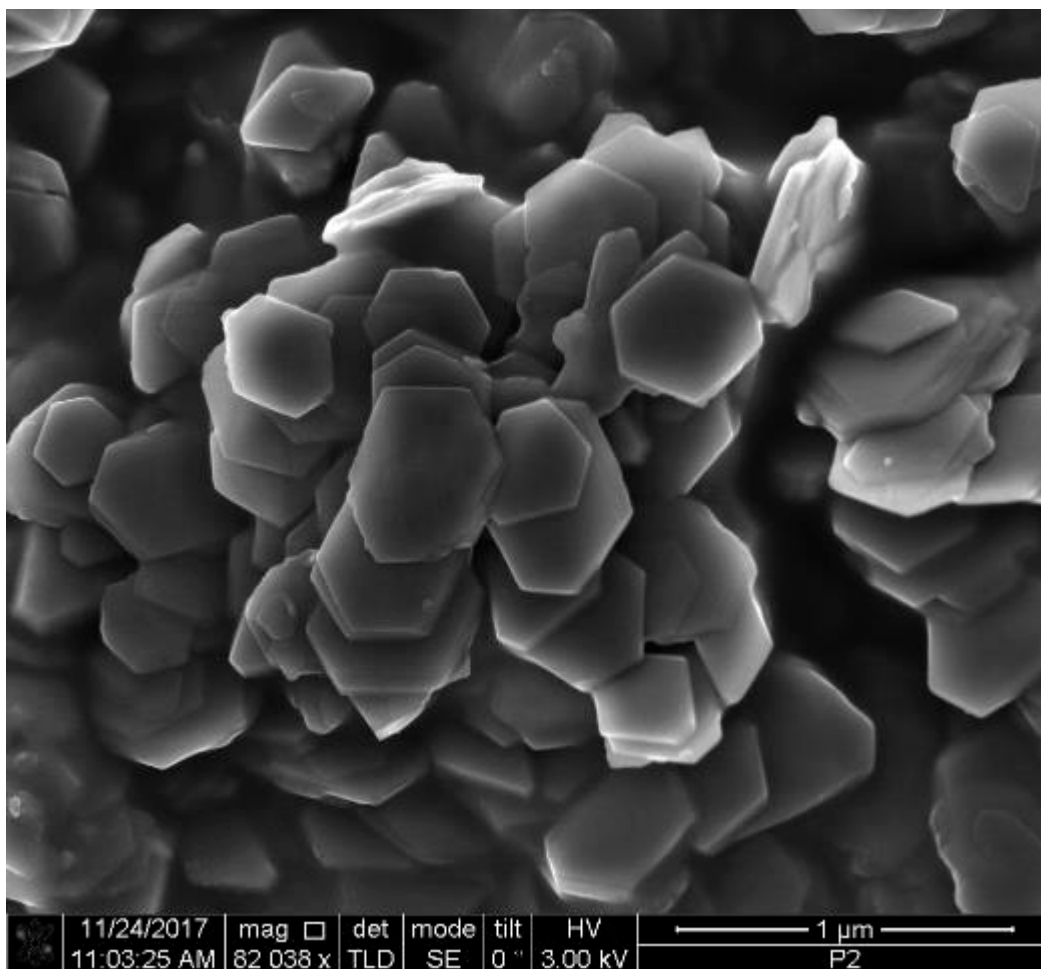


Figure 2. SEM of Gibbsite Solids Used in the Solubility Tests

3.2 Gibbsite Solubility Tests

To determine the solubility of gibbsite in the various test solutions, steady-state or equilibrium aluminum concentrations must be established. The guarantee of attainment of relatively unvarying aluminum concentration requires multiple samplings and analyses to verify that this condition is met. The attainment of steady-state aluminum concentrations in the tests from undersaturation and oversaturation is considered in the following two sections.

3.2.1 Attaining Steady-State Aluminum Concentration from Undersaturation

Tests of the solubility of nanoplate gibbsite as determined by dissolution of the solid (i.e., from undersaturation) were conducted in NaOH solutions containing varying concentrations of added NaNO_3 and NaNO_2 . The tests were performed at three temperatures—27 °C, 45 °C, and 80 °C—and measurements of the concentrations of aluminum were taken periodically to determine the approach to steady state or equilibrium. The attainment of a steady concentration was assessed by plotting the aluminum concentration data for each test as a function of time. The plateauing of the concentration values for at least three successive measurements was taken as evidence that equilibrium or steady-state had been reached. The tests were run up to 146 days of contact. However, due to the small particle size and high surface area of the gibbsite nanoplates, it was demonstrated in test T0 with 1 M NaOH and without other anions present that equilibrium in accordance with Misra (1970) was reached within one day. The test matrix with experimental conditions, based on actual masses of materials added and aluminum concentration findings, is shown in Table 3. The concentrations of NaNO_3 and NaNO_2 for the starting solutions, measured using ion chromatography (IC) analysis, differed by an average 5.3 +/- 4.4 % and 0.9 +/- 1.9 %, respectively, from the as-prepared solutions based on reagent masses (see Table B.1 in Appendix B).

Table 3. Experimental Conditions, Based on Masses of Materials Added, and Plateau Aluminum Concentration Findings in Molality (m) and Molarity (M)

Test	Temp., °C	[NaOH]		[NaNO ₃]		[NaNO ₂]		Average [Al], M	Std. Dev. [Al], M	Rel. Std. Dev., %
		m	M	m	M	m	M			
T0	27	1.01	1.01	0.00	0.00	0.00	0.00	0.083	0.001	2
T1	27	1.03	0.86	0.00	0.00	7.05	5.89	0.123	0.004	3
T2	27	1.03	0.89	4.91	4.23	0.00	0.00	0.106	0.003	3
T3	27	1.02	0.77	5.46	4.15	4.98	3.79	0.119	0.004	4
T4	27	6.07	6.03	0.00	0.00	0.00	0.00	0.758	0.047	6
T5	45	1.02	0.82	0.00	0.00	8.49	6.87	0.176	0.007	4
T6	45	1.04	0.86	6.34	5.25	0.00	0.00	0.145	0.007	5
T7	45	4.03	3.08	5.07	3.88	5.02	3.85	0.751	0.040	5
T8	45	6.11	6.06	0.00	0.00	0.00	0.00	1.009	0.046	5
T9	80	2.00	1.57	0.00	0.00	9.99	7.82	0.916	0.144	16
T10	80	1.98	1.57	7.97	6.32	0.00	0.00	0.787	0.176	22
T11	80	2.05	1.38	6.49	4.38	9.89	6.67	0.827	0.077	9
T12	80	6.15	6.11	0.00	0.00	0.00	0.00	2.262	0.276	12

The molar concentrations of aluminum measured in thirteen tests (T0-T12) are plotted in various test combinations in Figure 3–Figure 6. Evaluations of the equilibrium aluminum concentrations were performed to take into account all of the data in the indicated plateau interval and arrive at the stated average concentrations and associated standard deviations as given (Figure 3–Figure 6). These values, as well as the relative standard deviations (RSDs) of the aluminum concentration averages, are shown in

Table 3. The RSDs for the concentration measurements at 27 °C and 45 °C are 2% to 6%, whereas the 80 °C test RSDs range from 9% to 22%.

The higher variabilities observed for the triplicates at 80 °C tests may be due to greater variance in the temperature across the heating block at this higher temperature. It is also seen by visual examination of the data plots that for many of the tests at 80 °C (Figure 5 and Figure 6), later samples show greater variability in aluminum concentration. It is likely that the reaction vessel seal degraded over the longer timescale of the experiment, resulting in evaporation. Thus, the indicated plateau in Figure 5 and Figure 6 and the values in Table 3 demonstrate that the 80 °C tests reached equilibrium, but the later values are representative of more concentrated systems. Further consideration of the effect of time on the aluminum concentrations in the individual triplicate 80 °C tests is given in Appendix C.

The shapes of the aluminum concentration curves as a function of time are also informative. In all four of the 27 °C tests, the initial concentration measurements at 3 and 7 days trended upward, but did not exceed the plateau concentrations ultimately attained at 76 days. After that, at least for the tests run with 1 m NaOH (Figure 3), the aluminum concentrations fell, reaching their lowest measured values at 21 days, and then slowly rose before plateauing at about 76 days. The low concentration values at 21 days were about 80–85% of the final steady-state concentrations. Plots of the data versus the glovebox temperatures for these nominally 27 °C tests (Figure D.1 in Appendix D) indicate the aluminum concentrations roughly track, and increase, with the temperature. Thus, the temperature effect likely explains the variability. The steady-state concentrations were evaluated for tests T1, T2, and T3 at the four sampling times ranging from 76 to 135 days when the temperature averaged 27.7 °C (± 0.9 °C at one standard deviation). For the 27 °C test run with 6 m NaOH only (T4), an initial rise but no apparent dip in concentration was observed (Figure 6). Rather, after attaining the maximum concentration value at 7 days, steady-state concentration was reached at the next sampling at 10 days.

The shapes of the aluminum concentration curves for the 45 °C tests, T5 and T6 (with 1 m NaOH initially) and T7 (with 4 m initial NaOH), increase smoothly to reach steady state by 21 days (Figure 4). However, the approach to steady state covers a much larger relative aluminum concentration change for test T7, perhaps related to the larger quantities of gibbsite required to be dissolved to attain steady state. The average steady-state aluminum concentrations for these tests took into account five sampling times ranging from 21 to 84 days (Figure 4). Test T8, also run at 45 °C but with 6 m NaOH only (Figure 6), showed an aluminum concentration curve with time somewhat like that exhibited by the same test conditions at 27 °C (T4). The aluminum concentration in test T8 rose to reach its maximum at 15 days, and then slowly decreased to plateau at 35 days. The steady-state concentration value was evaluated using the data from the four samplings in the span from 35 to 84 days.

The aluminum concentrations for the three tests at 80 °C beginning with 2 m NaOH (T9, T10, and T11; see Figure 5) increased from the first sampling at 2 days until reaching steady concentrations at 27 days. The plateau aluminum concentration for T9 was evaluated for the three samplings at 27 to 56 days; the plateau aluminum concentration for tests T10 and T11 were evaluated using the four samplings at 27 to 83 days. After these times, the aluminum concentration values became more erratic (see Appendix C for further discussion). Test T12, beginning with 6 m NaOH only and run at 80 °C, showed the greatest variability of any of the tests within its triplicate analyses over its entire testing period (Figure 6). The aluminum concentrations still seemed to be rising after 2 days, but then settled, with relatively wide variability, for the four samplings at 6 to 42 days to provide the basis for estimating the steady-state aluminum concentration. The concentrations ranged much more widely in the ensuing three samplings, making any further evaluation of their meaning tenuous except to note the effects of water loss and temperature control.

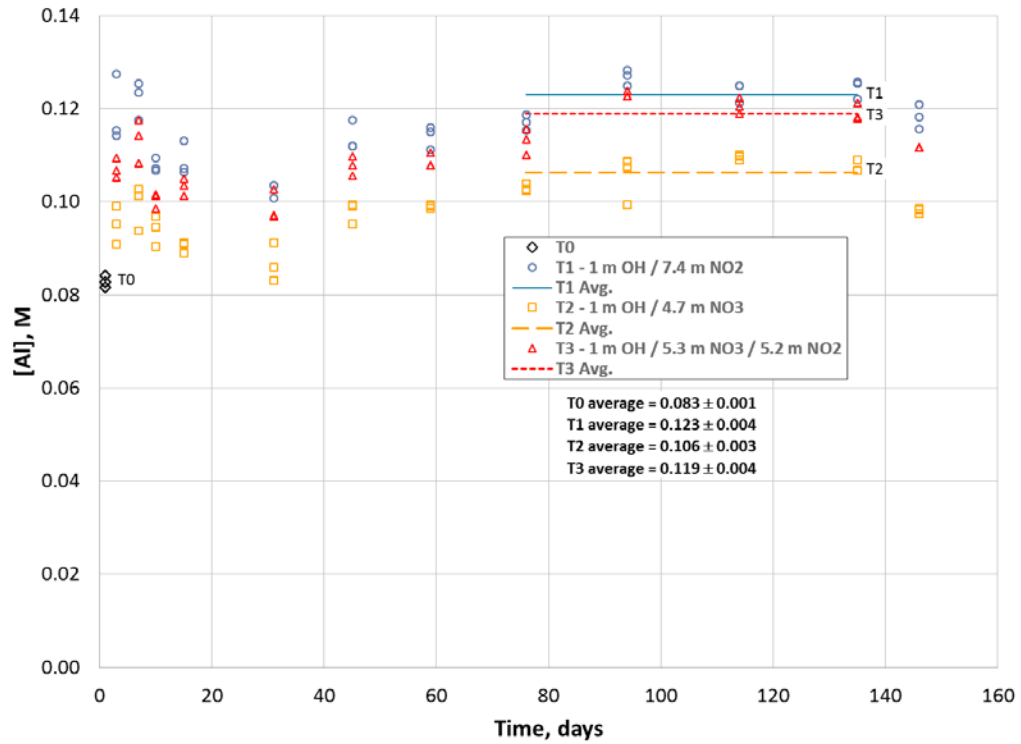


Figure 3. Gibbsite Solubility in 27 °C, 1 m NaOH Solutions with Varying [NaNO₃] and [NaNO₂]

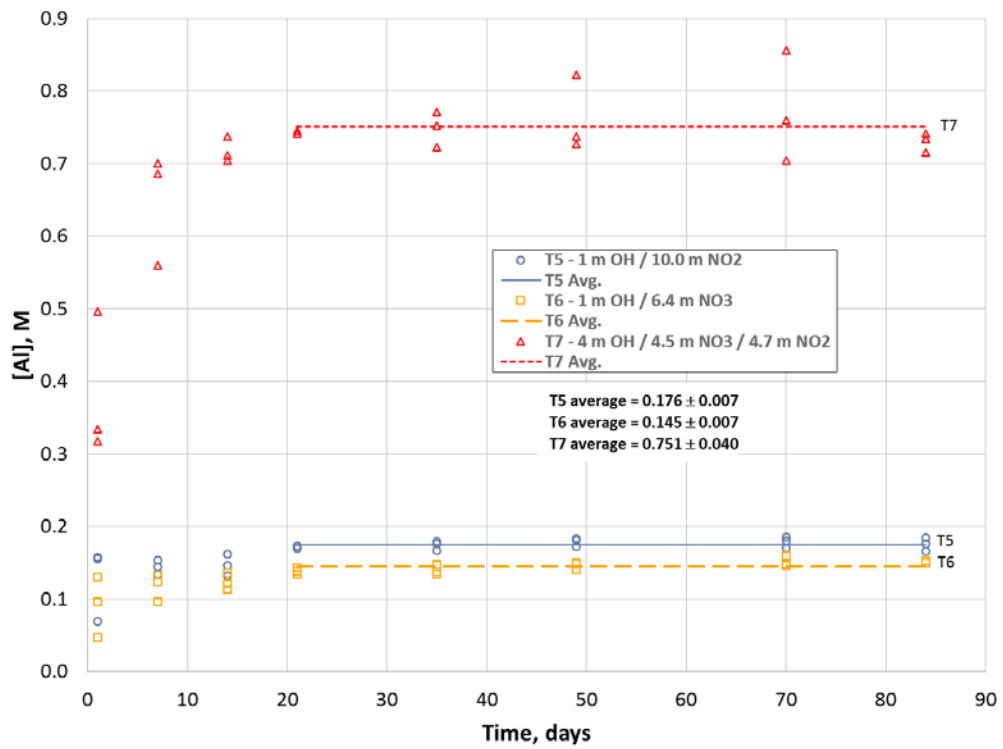


Figure 4. Gibbsite Solubility in 45 °C Tests with Varying [NaNO₃] and [NaNO₂] (T5 and T6 in 1 m NaOH; T7 in 4 m NaOH)

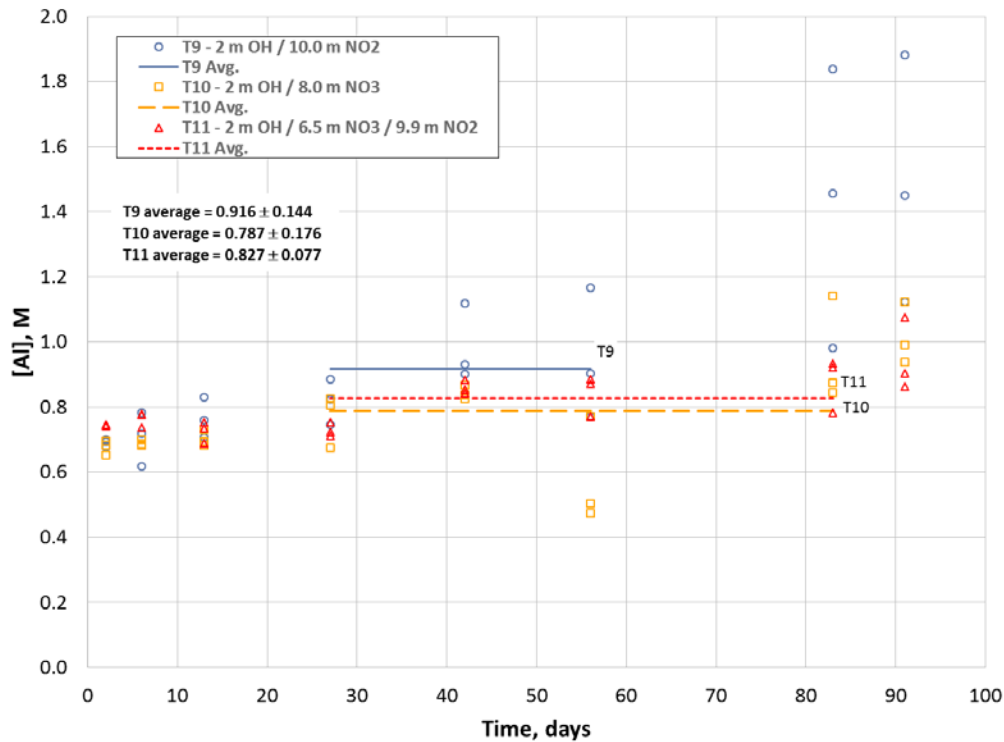


Figure 5. Gibbsite Solubility in 80 °C, 2 m NaOH Solutions with Varying [NaNO₃] and [NaNO₂]

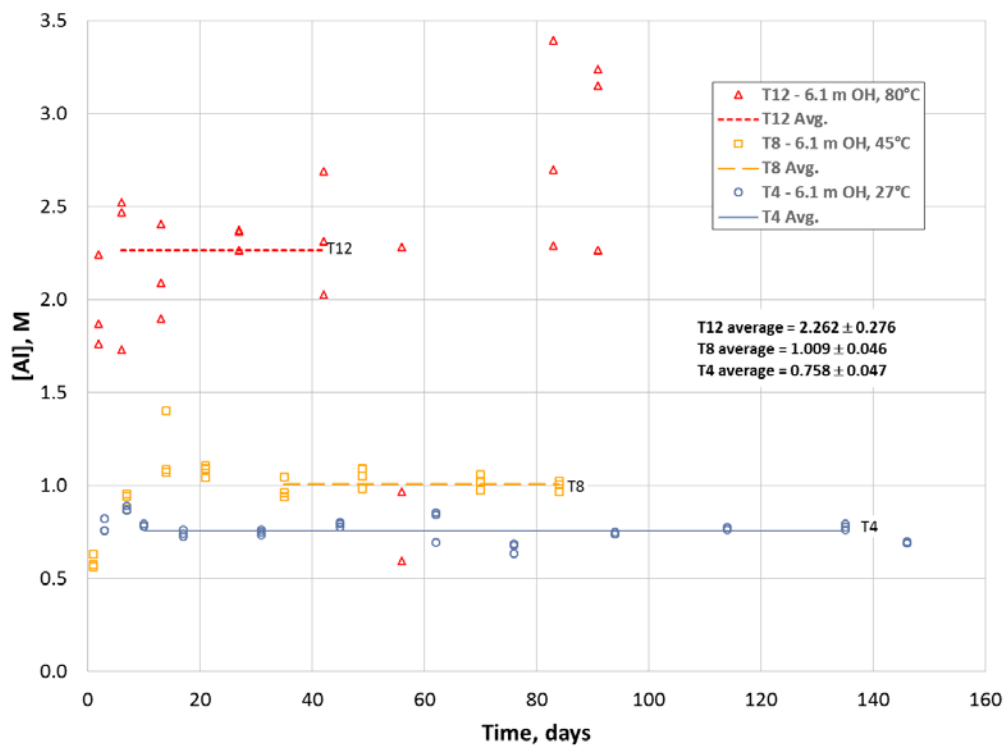


Figure 6. Gibbsite Solubility in 6 m NaOH Solutions at Varying Temperatures

3.2.2 Attaining Steady-State Aluminum Concentration from Oversaturation at 45 °C

Four paired tests of gibbsite dissolution from solid phase and precipitation from oversaturation were run at a 45 °C test temperature with identical initial solution compositions within each set. The tests within each set were T5 and T13, T6 and T14, T7 and T15, and T8 and T16. Each test was run in triplicate using the same respective starting solution. The nominal initial test solution compositions are shown in molality (m) and molarity (M) in Table 4, with molarity calculated using estimated 30 °C solution densities.

Table 4. Experimental Conditions for Tests at 45 °C Approaching Steady State from Undersaturation and Oversaturation

Test Number	Temperature, °C	Make-up Concentration					
		Molality, m			Molarity, M		
		NaOH	NaNO ₃	NaNO ₂	NaOH	NaNO ₃	NaNO ₂
T5	45	1.02	0.00	8.49	0.82	0.00	6.87
T13	80→45	1.01	0.00	8.85	0.81	0.00	7.10
T6	45	1.04	6.34	0.00	0.86	5.25	0.00
T14	80→45	1.00	6.15	0.00	0.83	5.12	0.00
T7	45	4.03	5.07	5.02	3.08	3.88	3.85
T15	80→45	4.03	5.20	5.09	3.07	3.96	3.88
T8	45	6.11	0.00	0.00	6.06	0.00	0.00
T16	80→45	6.09	0.00	0.00	6.04	0.00	0.00

The tests from undersaturation (T5, T6, T7, and T8) were mixed with excess nanoplate gibbsite solids and placed in 45 °C thermostatted heating blocks with stirring. The tests from oversaturation also were mixed with excess nanoplate gibbsite (at the rate of not less than 1.5-times the expected gibbsite solubility at 45 °C) and heated overnight to 80 °C when a clear solution was obtained. The solutions then were cooled to 45 °C and the temperature was maintained using a heater block with stirring. The temperatures for these tests (T13, T14, T15, and T16) are indicated by 80→45. The solutions in each test were sampled periodically and analyzed by ICP for aluminum concentration. For tests T13 and T16, no crystallization or decrease in aluminum concentration was observed in any of the triplicates after 37 days, and prior to the addition of more gibbsite nanoplates as seed crystals (Figure 7 and Figure 10, seeding denoted by red arrow). For test T14, two of the triplicates developed turbidity after 32 days, accompanied by an ~15% decrease in aluminum concentration, compared with the triplicate that showed no obvious crystallization (Figure 8, seeding denoted by red arrow). For test T15, one of the triplicates developed turbidity after 32 days, accompanied by an ~21% decrease in aluminum concentration, compared with the two triplicates that showed no obvious crystallization (Figure 9, seeding denoted by red arrow). These results highlight that the oversaturated solutions are thermodynamically unstable, and even small fluctuations in solution conditions between the triplicate samples are enough to overcome the kinetic barrier to crystallization in some cases. After 76, 49, 49, and 66 days, respectively, for tests T13, T14, T15, and T16, additional nanoplate gibbsite (0.4 g) was added to each test to act as seed crystals, as denoted by the red arrow in Figures 7 through 10.

The plotted data include the concentration values for all of the triplicate runs and give some idea of the experimental scatter. Despite the scatter (perhaps due to small differences in the temperature), it can be seen that the 45 °C tests run from undersaturation reached steady concentrations within about 20 to 30 days.

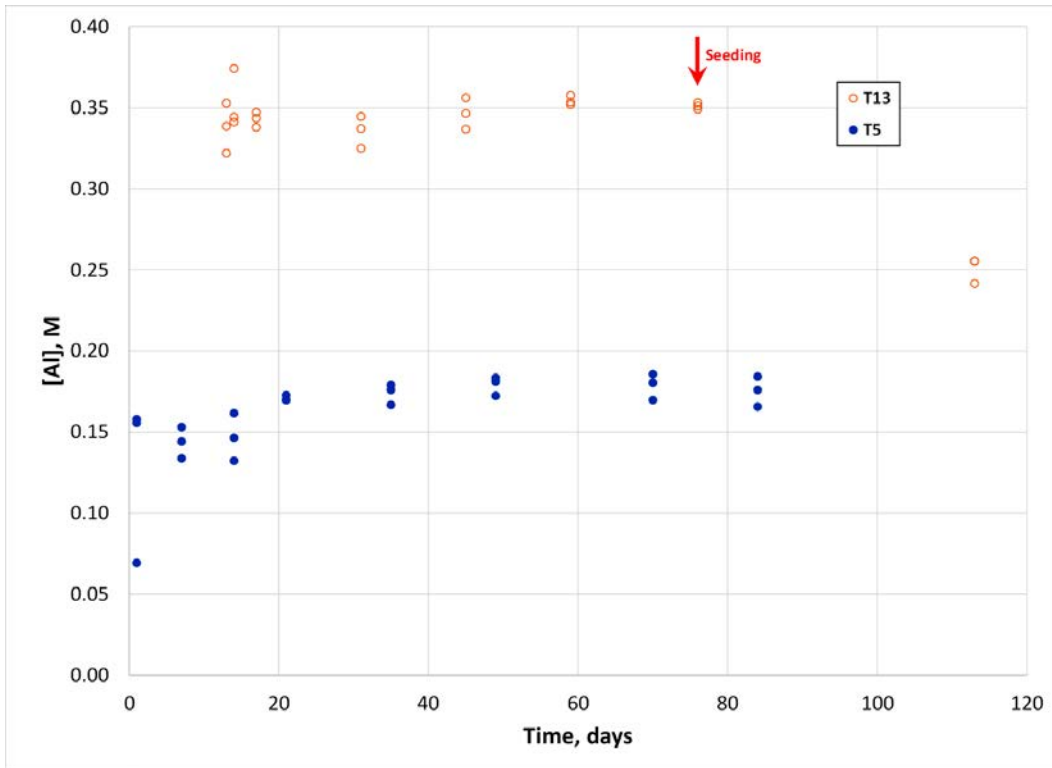


Figure 7. Aluminum Concentrations versus Time for Tests T5 and T13

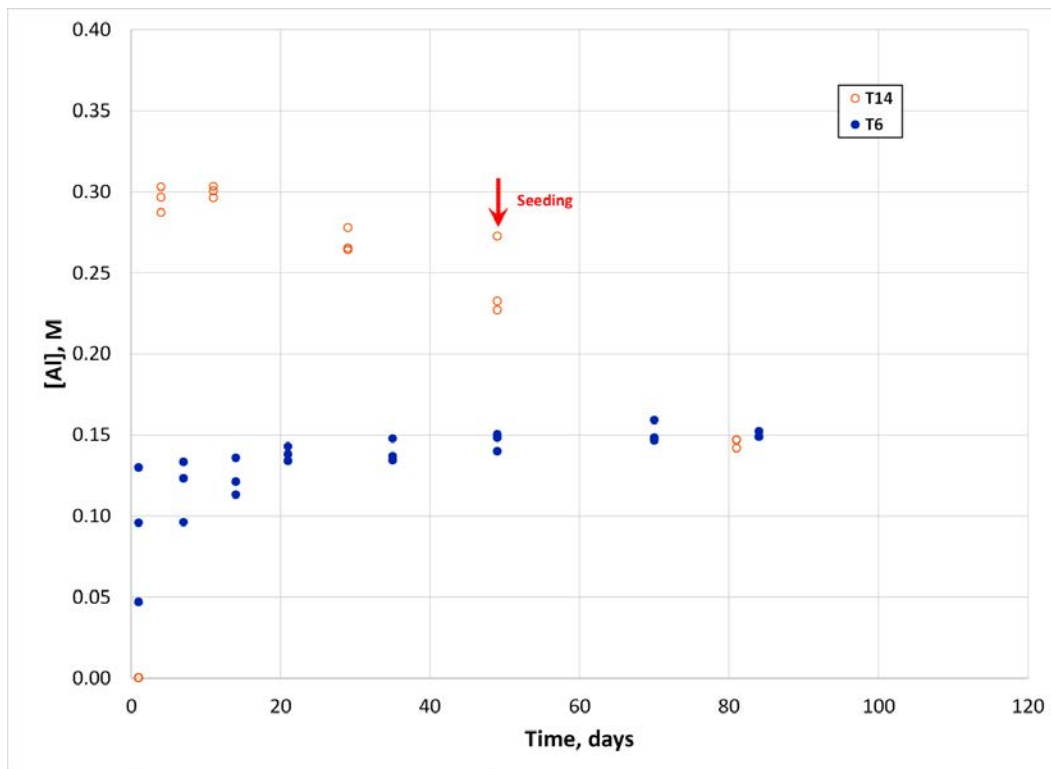


Figure 8. Aluminum Concentrations versus Time for Tests T6 and T14

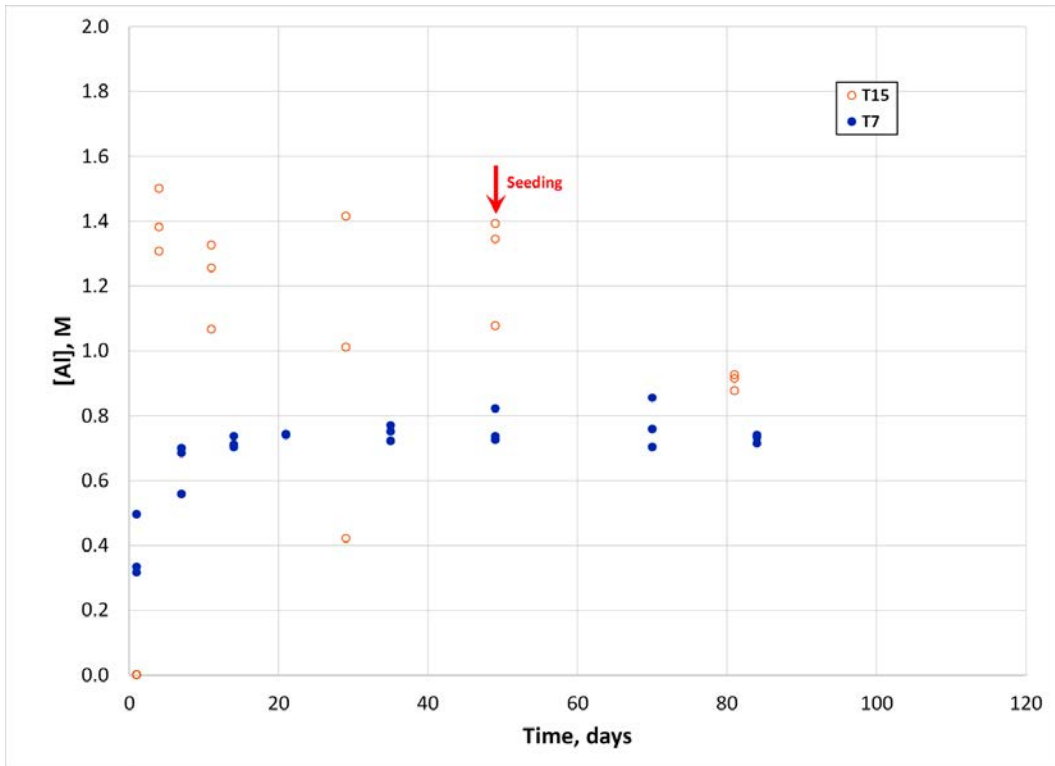


Figure 9. Aluminum Concentrations versus Time for Tests T7 and T15

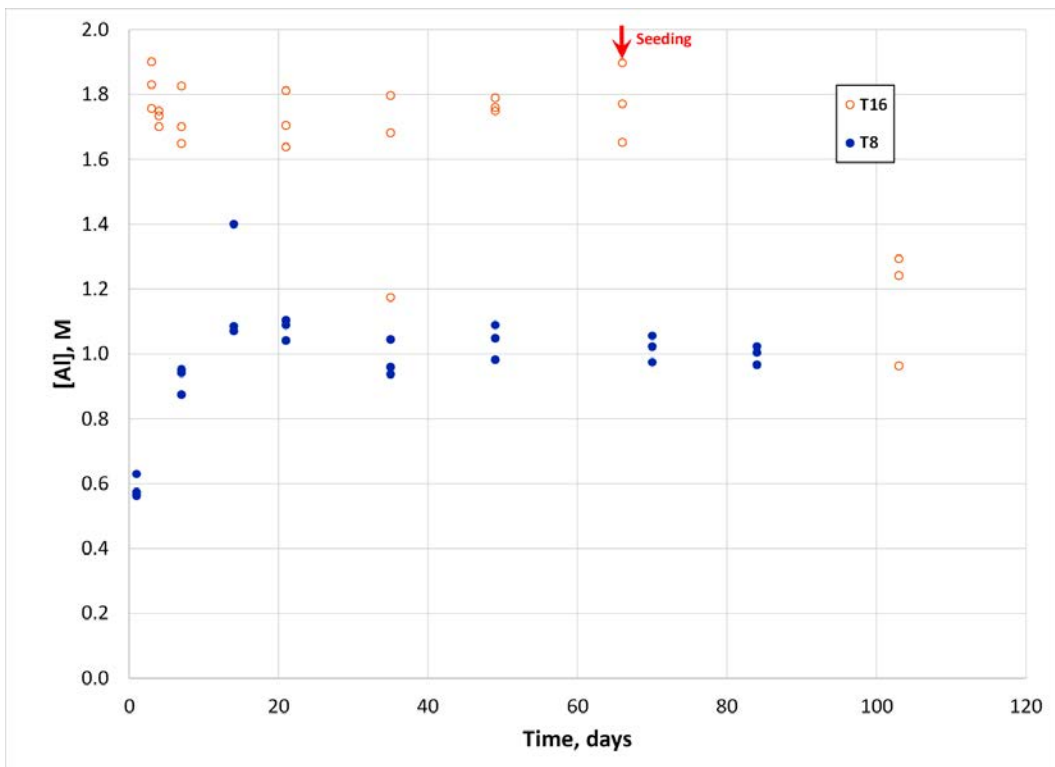


Figure 10. Aluminum Concentrations versus Time for Tests T8 and T16

The tests from oversaturation began with aluminum concentrations approximately double the observed steady-state concentrations of the corresponding tests from undersaturation. It is evident that many of the tests from oversaturation were able to maintain their oversaturated condition for extended times. After the addition of the seed gibbsite at 49 to 76 days and subsequent equilibration for about one month, the aluminum concentrations matched (or approached) those attained within the similar 20–30 days for the tests from undersaturation.

The high specific surface area of the gibbsite nanoplates likely led to the attainment of steady state in aluminum concentration from undersaturation within 20–30 days. At the same time, the ability of a sodium aluminate solution to remain supersaturated in gibbsite is clearly demonstrated for the 80→45 tests.

Thus, the parallel 45 °C tests approached or achieved convergence in aluminum concentration within about one month after seeding, but remained at supersaturation before seeding (and roughly two-fold above equilibrium solubility) for about two months. Comparison of the data shows, however, some downward trending of aluminum concentration toward equilibrium for those tests containing nitrate (i.e., tests T14 and T15), along with observed turbidity in some of the triplicates, highlighting the thermodynamic instability of these systems.

Overall, gibbsite solubility, as measured by aluminum concentration, increases by a factor of ~3 (at 5.95 M initial NaOH) as temperature increases from 27 to 80 °C (Figure 6).

3.2.3 Measured Gibbsite Solubility in Current Tests versus Misra (1970) Predicted Solubility

The Misra Equation [Equation (1)] summarizes gibbsite solubility observations from numerous studies and provides a useful gibbsite solubility relationship for NaOH-NaAl(OH)₄ solutions in equilibrium with gibbsite as a function of temperature. Thus, Equation (1) was used in this study to predict Al solubility in molarity as a function of the test conditions in Table 2. The achievement of steady-state aluminum concentrations in tests T1 through T12 is shown in Figure 3 through Figure 6; attainment of the steady-state concentrations for the 80→45 °C tests (from oversaturation) is demonstrated in Figure 7 through Figure 10. However, the hydroxide concentrations in these test items were only measured at the completion of the contact times, well after steady states were reached. The measured temperature, density, and equilibrium concentrations of OH⁻, NO₂⁻, NO₃⁻, and Al(OH)₄⁻ in molarity at these final samplings are given in Table D.1 of Appendix D and are considered to be at equilibrium as demonstrated by their earlier attainment of steady-state concentrations. The density and molar concentration values were used to derive, by calculation, the corresponding molal concentrations for OH⁻, NO₂⁻, NO₃⁻, and Al(OH)₄⁻; these values are also found in Table D.1. Values are provided for each of the three triplicates run at each test condition. For the tests at 80 °C (T9–T12), the final values for solubility provided in Table D.1 represent a more concentrated system than the equilibrium values in Table 3 due to evaporation and water loss from the solutions, which increases the residual NaOH concentration and favors gibbsite dissolution. However, as shown in Figure 3, due to the small particle size and high surface area of the gibbsite nanoplates, equilibrium is reached very rapidly (within one day), so the aluminum concentrations represent the equilibrium values for the test conditions, in terms of hydroxide concentration as determined by acid titration, and nitrate/nitrite concentrations as determined by IC analysis (provided in Table D.1).

According to the Misra Equation, the gibbsite solubility increases by a factor of ~28 as NaOH concentration increases from 0.4 to 5 M at 25 °C and increases by about a factor of 5 (at 1 M NaOH) as temperature increases from 27 to 80 °C (Figure 11). However, the temperature effect is markedly greater at higher NaOH concentrations, with aluminum concentration rising more steeply as NaOH concentration

increases. The data surveyed for Equation (1) ranged from 25 to 100 °C and goes up to 230–240 g Na₂O/L (i.e., total sodium concentration of ~7.5 M in the NaOH-NaAl(OH)₄ system). T4, T8, T12, and T16 with no added NO₃⁻ or NO₂⁻ nitrate or nitrite all began with 6 m (~6 M) initial NaOH, equivalent to ~186 g Na₂O/L, so these tests are in the alkaline sodium (salt excluded) concentration range of validity of the data supporting Equation (1). Tests T1, T3, T5, T7, T9, T11, T13, and T15 have sodium concentrations that exceed the validated range of Equation (1), but not in terms of the sodium as alkalinity associated with OH⁻ and Al(OH)₄⁻. As noted by the author (Misra 1970), Equation (1) over-predicts or under-predicts experimental trends under certain conditions, with the scatter due to the differences intrinsic in the various experimental set-ups in the surveyed studies and also differences between approaching equilibrium from over- or undersaturation.

For tests T0, T4, and T8 (i.e., those tests from undersaturation without added NaNO₃ or NaNO₂), there is good agreement between the Al(OH)₄⁻ concentration predicted by Equation (1) and the measured Al(OH)₄⁻ concentration at 27 °C and 45 °C at ~6 m initial hydroxide concentration (Figure 11, open circles) and 27 °C at 1 m initial NaOH, although many values were trending somewhat below the Misra Equation. For test T12 at 80 °C, the Al(OH)₄⁻ concentration is below that predicted by Equation (1); however, at this concentration of hydroxide, we are approaching the limits of the Misra (1970) equation. In Misra (1970), there are relatively few data for ~70–100 °C at ~6 M NaOH (total), equivalent to 186 g Na₂O/L, and the data given (mostly at 95 °C and 100 °C) are lower than the line predicted by the Misra Equation. In addition, data from other studies (e.g., Bénézeth et al. 2016) also trend below that predicted at high temperatures and hydroxide concentrations (see Figure 12), suggesting that Equation (1) does not accurately predict aluminum solubility under these more extreme conditions.

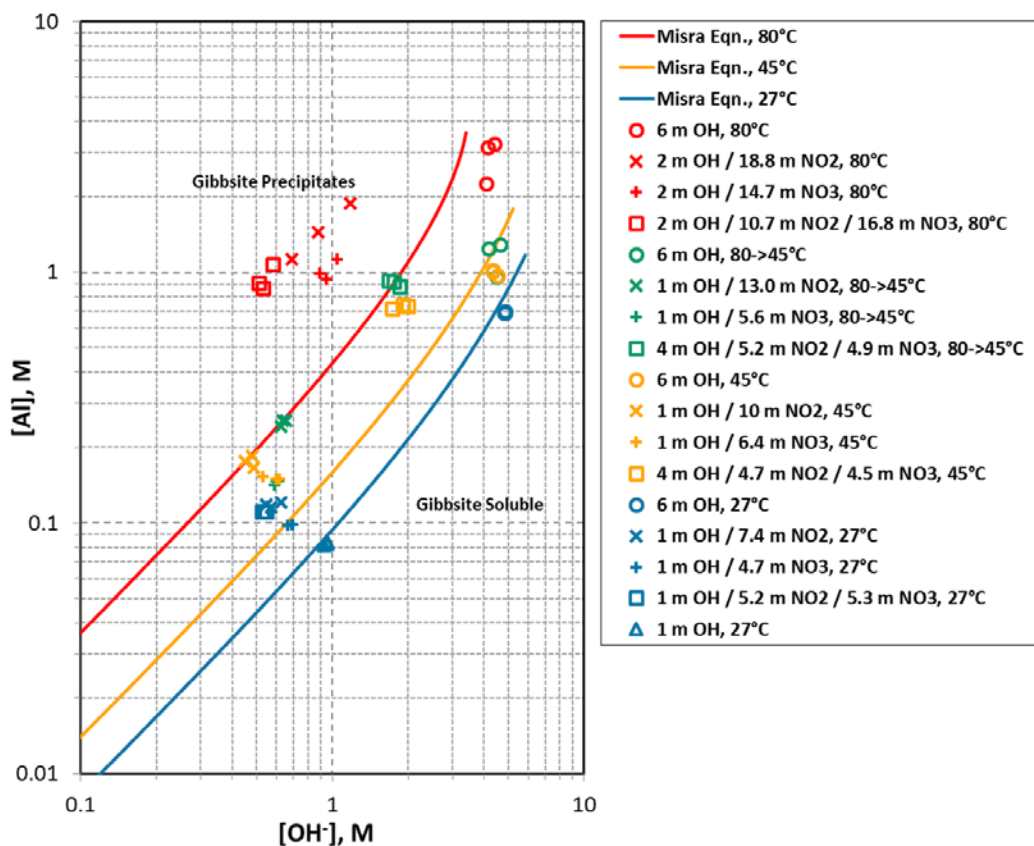


Figure 11. Measured Gibbsite Solubility in Current Tests versus Misra Equation Predicted Solubility in NaOH Solutions as Functions of NaOH Concentration and Temperature

3.2.4 Measured Gibbsite Solubility in Current Tests in Molality Units

While it is convenient to compare gibbsite solubility in molarity units for $\text{NaNO}_3/\text{NaNO}_2$ -containing solutions with that predicted by the Misra Equation, and also with prior Hanford and non-Hanford studies, (Delegard 2018), this presents a problem because the difference in the density of the $\text{NaNO}_3/\text{NaNO}_2$ solution is superimposed on the observed thermodynamic differences. For example, the difference in gibbsite solubility in the NaNO_2 -containing solutions compared to that predicted by the Misra Equation in molarity units, as shown in Figure 11, may simply be due to the density difference between solutions containing NaNO_2 versus NaNO_2 -free solutions. Therefore, a comparison must also be made in molality units.

The data for the 27 °C tests (T0, T1, T2, and T3) demonstrates that the added $\text{NaNO}_3/\text{NaNO}_2$ certainly increases the density of the nominal initial 1 m NaOH solutions (Table D.1). However, the added $\text{NaNO}_3/\text{NaNO}_2$ also decreases the free hydroxide molality in these parallel tests (T1–T3) by the corresponding increase in the aluminum molality compared with the $\text{NaNO}_3/\text{NaNO}_2$ -free test (T0). Therefore, on a molality basis, the aluminum concentration (0.109 to 0.146 m) in the solutions containing $\text{NaNO}_3/\text{NaNO}_2$ (T1–T3) is higher at a lower free hydroxide (0.644 to 0.775 m) than the aluminum concentration (0.079 to 0.081 m Al in 0.898 to 0.925 m free hydroxide) in the $\text{NaNO}_3/\text{NaNO}_2$ -free solution (T0). The total alkalinity in tests T1, T2, and T3 is lower than in T0. Figure 12 and Figure 13 clearly show that gibbsite is more soluble in solutions containing $\text{NaNO}_3/\text{NaNO}_2$ than in $\text{NaNO}_3/\text{NaNO}_2$ -free solutions at approximately the same total alkalinity, and when expressed in molality units. Additional evidence for the effect of $\text{NaNO}_3/\text{NaNO}_2$ on gibbsite solubility is provided in the plot of gibbsite solubility versus temperature (Figure D.1 in Appendix D), which shows, in addition, that the solubility sensitivity to temperature is greater in solutions containing $\text{NaNO}_3/\text{NaNO}_2$ than in $\text{NaNO}_3/\text{NaNO}_2$ -free solutions.

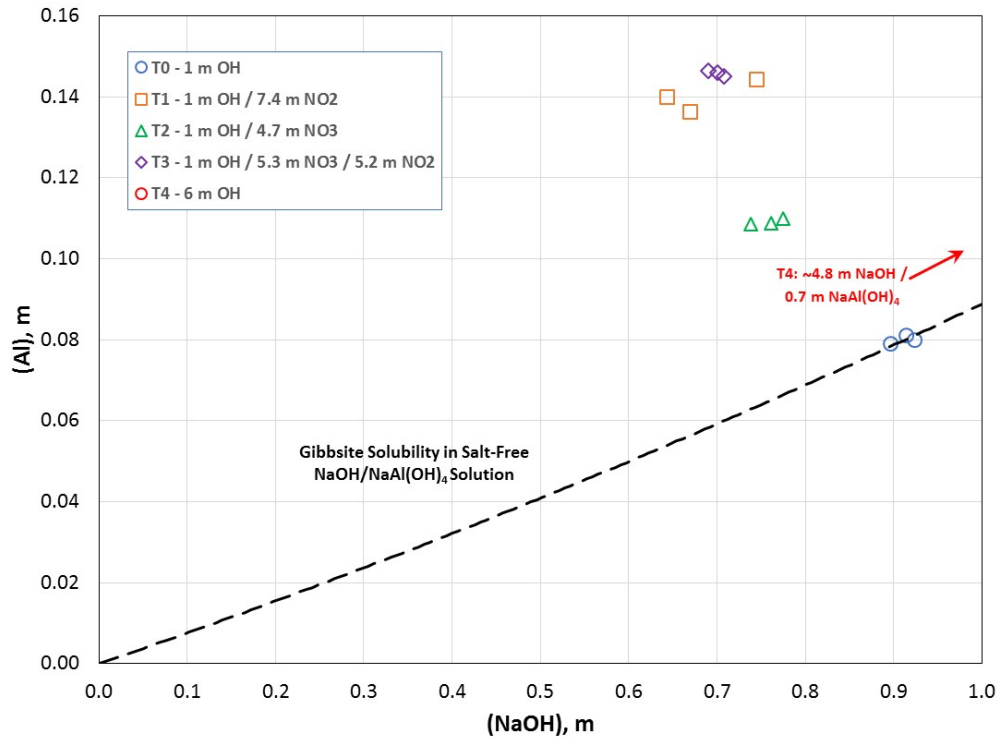


Figure 12. Measured Gibbsite Solubility in 27 °C Tests with ~ 1 m NaOH (T0-T3) with Hydroxide and Aluminum Concentrations Expressed in Molality Versus Predicted Solubility in $\text{NaNO}_3/\text{NaNO}_2$ -free $\text{NaOH}/\text{NaAl}(\text{OH})_4$ Solutions as Functions of NaOH Concentration

Figure 12 also shows that the gibbsite solubility is not solely influenced by the ionic strength (i.e., sodium concentration), as gibbsite solubility in T1 (containing 8.09 m sodium) is considerably higher than in T2 (containing 5.97 m sodium), but gibbsite solubility in T3 (containing 11.46 m sodium) is not significantly higher than T1. This suggests that it is the anion (NO_3^- or NO_2^-) that plays the major role in influencing gibbsite solubility by the addition of NaNO_3 and NaNO_2 .

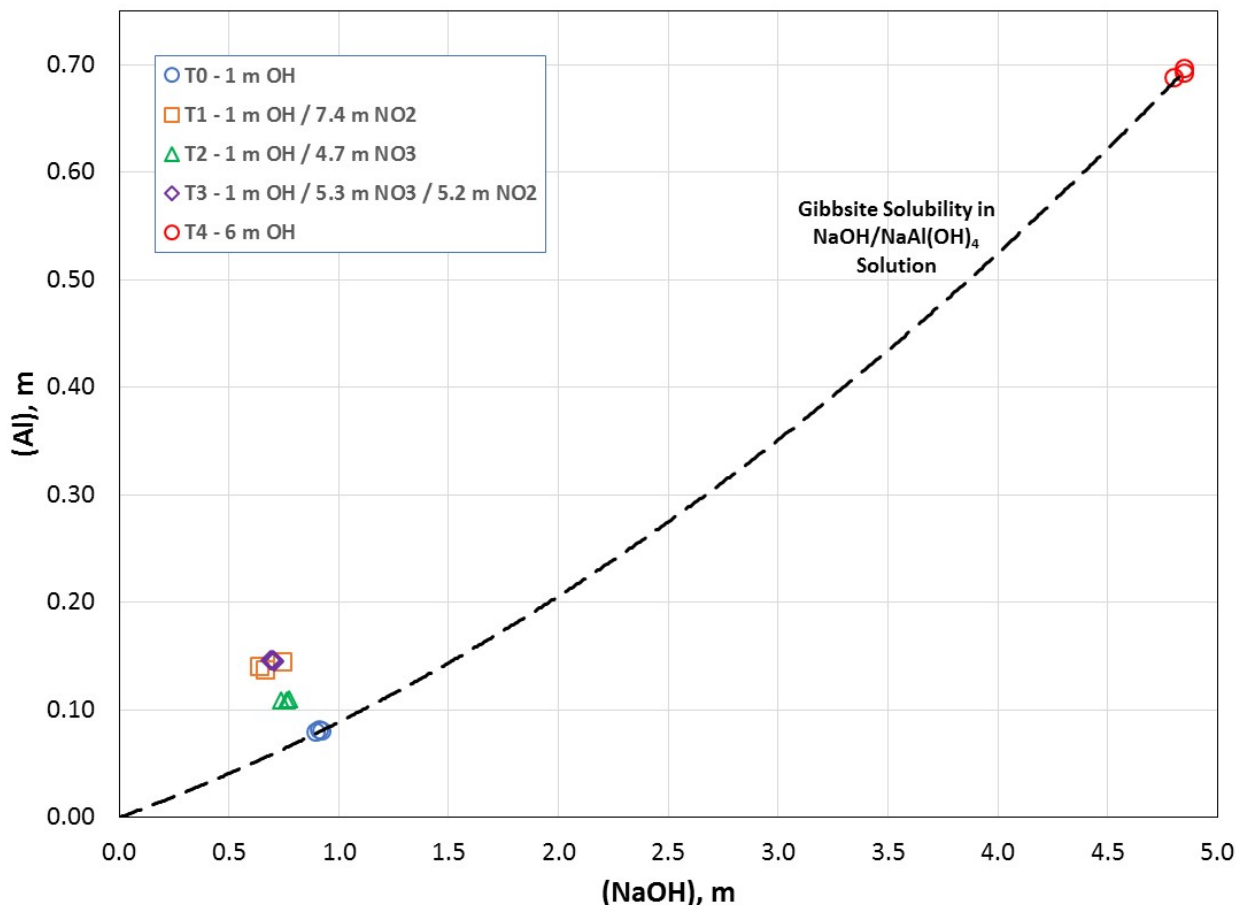


Figure 13. Measured Gibbsite Solubility in 27 °C Tests (T0-T4) with Hydroxide and Aluminum Concentrations Expressed in Molality Versus Predicted Solubility in NaNO₃/NaNO₂-free NaOH/NaAl(OH)₄ Solutions as Functions of NaOH Concentration

3.2.5 Gibbsite Solubility in NaOH-NaAl(OH)₄-NaNO₃ Solutions

In this system, NaNO₃ was added to the NaOH-NaAl(OH)₄ solutions in T2, T6, T10, and T14 at 27 °C, 45 °C, and 80 °C from undersaturation, and at 80 °C cooled to 45 °C from oversaturation, respectively. The added NaNO₃ concentrations at the end of the experiments ranged from about 4.0 to 9.6 M and the final free NaOH concentrations ranged from 0.63 to 2.0 M. The time taken to reach equilibrium, determined as steady aluminum concentration, was only days, but sampling for aluminum concentration continued for up to 146 days, with measurements made for all component concentrations using solutions from the final samplings.

Gibbsite solubility data for the relatively high NaNO₃ concentrations used in these solutions may be compared with literature data trends at lower NaNO₃ concentrations (3 M and below). The higher NaNO₃ concentrations used in the present tests thus extend knowledge of this system beyond that provided in the technical literature. In the present tests, the addition of NaNO₃ increased gibbsite solubility over the temperature range of 27 to 80 °C in tests run from both undersaturation and oversaturation. In solutions containing 0.8 to 1.5 M NaOH and 4.3 to 7.5 M NaNO₃, the equilibrium Al concentrations were ~1.2- to 2.2-times higher than those predicted by the Misra Equation for the simple NaOH-NaAl(OH)₄ system at the same free hydroxide concentration but containing no additional salt. The impact was greater for

increased nitrate concentration and temperature, but the source of the impact is confounded because the tested nitrate concentrations were increased for the higher test temperatures.

The parallel 45 °C NaOH/NaNO₃ tests from undersaturation (T6) and from oversaturation in gibbsite (T14) converged in aluminum concentration but only after seeding. It is evident, however, that even before seeding, the aluminum concentrations from oversaturation began trending downward slowly after approximately 11 days (Figure 8).

The findings in the technical literature for the NaOH-NaAl(OH)₄-NaNO₃ system are described in the following paragraphs. At least four studies have been undertaken to determine the solubility of gibbsite in NaOH-NaAl(OH)₄-NaNO₃ solutions.

In the first study, the solubility equilibrium was approached at 25 °C from undersaturation by dissolution of excess water-washed, and otherwise undescribed, Al(OH)₃ (Felmy et al. 1994). Tests were run at 0.1, 0.5, 1, and 3 M initial NaOH. The testing showed gibbsite solubilities to be nearly independent of NaNO₃ concentration (ranging up to 8 m); the solubilities reached steady state (equilibrium) in less than six days for the lower NaOH concentrations, but took over a year to equilibrate in the 3 M NaOH tests. This longer time was attributed to the extent of dissolution required for these more concentrated solutions and may indicate that the starting gibbsite was of relatively low specific surface area. Solid phase characterization by XRD at the end of testing confirmed the solid phase to be gibbsite.

The second study (Bénézeth et al. 2016) was similar to the first (Felmy et al. 1994), approaching equilibrium from undersaturation in the presence of excess Al(OH)₃, but run at 30 °C, 63 °C, and 89.8 °C. The NaNO₃ concentrations ranged from 0 to ~4 M and the initial NaOH concentrations ranged up to ~4 M, but combinations of high (>1 M) concentrations in both were scarce. The gibbsite used was obtained from Alcoa, Inc. (C-33); the BET surface area was 0.36 m².g⁻¹, with no detectable particles below 1 μm and greater than 95% of the material in the 10-35 μm range. Equilibrium in all tests was reached within 20 days.

Concentrations were reported in molal in both data sets. To be consistent with other reported data [e.g., in Tank Waste Information Network System (TWINS)] and with the Misra Equation, the concentrations were converted to molarity, at 30 °C, by using a solution density prediction equation (Orme 2003) and iteration until convergence in molar concentrations was obtained for hydroxide, aluminate, and nitrate. The gibbsite solubilities obtained by the Felmy et al. (1994) and Bénézeth et al. (2016) experiments are compared in Figure 14 with the solubilities predicted using the Misra Equation at the same temperatures and NaOH molar concentrations. It is seen that, within the individual tests in the Felmy et al. (1994) and Bénézeth et al. (2016) studies, added nitrate had a small positive effect on gibbsite solubility in the 25 °C and 30 °C experiments. However, the observed concentrations are still very near those found in the Misra fit of the simple NaOH-NaAl(OH)₄ solutions. Even at the higher temperatures (63 °C and 89.8 °C), only a small increase in aluminum concentration ensued as a result of the added NaNO₃, even though little difference is seen at higher temperatures between the observations of Bénézeth et al. (2016) and the predictions based on the Misra Equation.

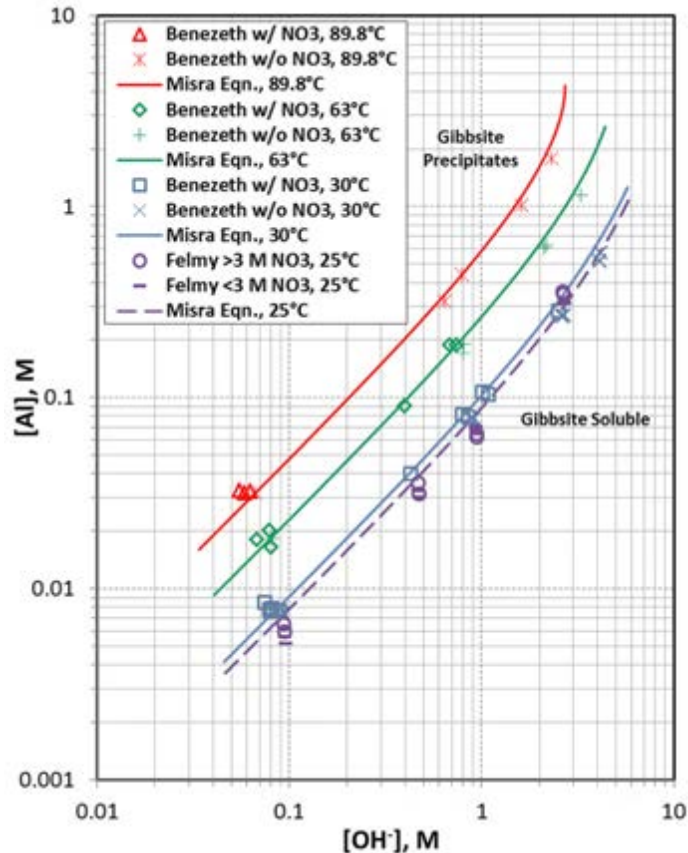


Figure 14. Gibbsite Solubility in the Presence of NaNO_3 (Felmy et al. 1994 and Bénézeth et al. 2016)

The third study investigated the dissolution of gibbsite in 3 M NaOH containing 0, 1, 2, and 3 moles of NaNO_3 per kilogram of NaOH solution to determine the effects of nitrate on the gibbsite dissolution steady-state concentration (Russell et al. 2009). The gibbsite used was Almatris C333 and had specific surface area of $4.8 \text{ m}^2/\text{g}$, particle size, by number, of about 85% less than $1 \mu\text{m}$ and 50 vol% less than $5.88 \mu\text{m}$. Because solution densities were measured, concentrations could be calculated in molarity. The tests were run in duplicate at nominal room temperature (stated to be $\sim 20^\circ\text{C}$) and appeared to reach steady aluminum concentrations after about 15 days. Separate tests of the precipitation of gibbsite-seeded supersaturated solutions at room temperature ($\sim 20^\circ\text{C}$) started with the same initial NaOH and NaNO_3 concentrations. The supersaturated solutions were prepared by dissolving gibbsite at 100°C for eight hours. Additional fresh gibbsite was added and the solutions allowed to cool. The solution concentrations were monitored for 30 days, by which time the concentrations appeared to be reaching, though not quite attaining, asymptotic values.

A fourth study, whose other results are examined in further detail later in this report (Herting 2014), investigated gibbsite dissolution in 22°C NaOH solution with and without added NaNO_3 . These tests by Herting (2014) used much coarser Almatris C33 gibbsite starting material as compared with the tests by Russell et al. (2009). The Almatris C33 gibbsite had $0.545 \text{ m}^2/\text{g}$ specific surface area, less than 1%, by number, particles less than $1 \mu\text{m}$, and 50 vol% of the particles less than $60.4 \mu\text{m}$ (Russell et al. 2009). The solution concentrations were measured for five or ten weeks, depending on the test. The aluminum concentrations for most tests, however, failed to reach steady aluminum concentration within the five or ten week test durations. The coarser gibbsite particle size used in Herting's (2014) tests may explain the relatively slow attainment of steady-state aluminum concentration. To forecast the steady-state concentrations, the aluminum concentration versus time data were fit to asymptotic curves. It was found

that the aluminum concentrations at the final samplings at five or ten weeks were from 68% to 87% of the projected “equilibrium” values.

The results of the third and fourth test series (Russell et al. 2009; Herting 2014) are compared in Figure 15, with the solubility predicted for the simple NaOH-NaAl(OH)₄ system according to the Misra Equation. For both Russell et al. (2009) and Herting (2014) test sets begun from undersaturation, concentrations were near those anticipated by the Misra Equation. However, for both, the addition of sodium nitrate enhanced aluminum concentration in a clear consistent manner. In the tests by Russell and colleagues (2009), the gibbsite solubility increased about 0.11 M, or about 50%, relative, as NaNO₃ concentration increased from 0 to 2.88 M. For Herting (2014), the aluminum concentration around 3 M NaOH was projected (using the Misra 1970 line slope) to be about ~0.08 M greater with 3 M NaNO₃ present than with NaNO₃ absent.

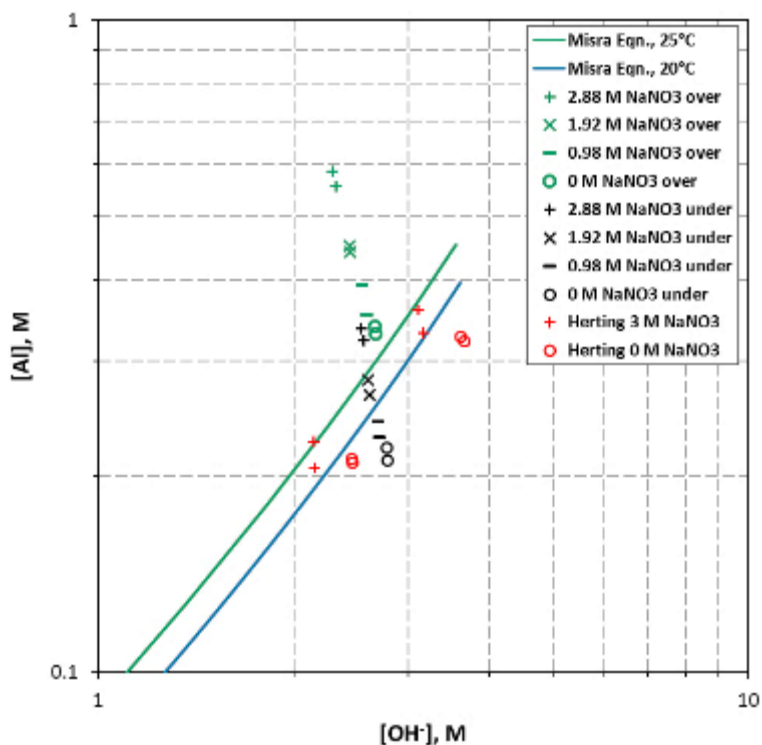


Figure 15. Gibbsite Solubility in the Presence of NaNO₃ at Near Room Temperature in Tests from Both Undersaturation and Oversaturation (Russell et al. 2009 and Herting 2014)

The aluminum concentrations in the oversaturation tests by Russell et al. (2009) had reached nearly steady concentrations by 30 days of contact, but appeared to still be very slowly decreasing. Nevertheless, as shown in Figure 15, the concentrations remained about 1.6-times higher than in the tests run from undersaturation. The relative disparities between the under- and oversaturation results increased with NaNO₃ concentration.

The disparity of the apparent gibbsite solubility tests, with higher concentration observed for tests run from oversaturation than from undersaturation, was observed both in the present experiments for all tested systems—NaOH only, NaOH-NaNO₃, NaOH-NaNO₂, and NaOH-NaNO₃-NaNO₂—and in the tests by Russell et al. (2009).

3.2.6 Gibbsite Solubility in NaOH-NaAl(OH)₄-NaNO₃-NaNO₂ Solutions

Both NaNO₃ and NaNO₂ were added to the NaOH-NaAl(OH)₄ solutions in T3, T7, T11, and T15 at 27 °C, 45 °C, and 80 °C from undersaturation, and at 45 °C from oversaturation, respectively. The NaNO₃ and NaNO₂ concentrations ranged from about 3.5 to 8 M at the end of testing, and the final NaOH concentrations ranged from 0.5 to 2 M. The time taken to reach equilibrium from undersaturation was only days but tests were allowed to continue up to 143 days before final sampling. The addition of NaNO₃ and NaNO₂ had a positive effect on gibbsite solubility over the temperature range of 27 to 80 °C in tests run from undersaturation. In the 27 °C and 45 °C tests from undersaturation, each contained approximately 3.5 to 4 M in both NaNO₃ and NaNO₂; the Al concentrations were about two times those predicted by the Misra Equation. This positive effect on equilibrium Al concentration was similar for T15, the 45 °C test from oversaturation. The solubility enhancement was about four-fold for the undersaturation test run at 80 °C, which contained ~4.8 M NaNO₃ and 8 M NaNO₂ by the end of the test.

The solubilities of gibbsite and the sodium salts NO₃⁻, NO₂⁻, sulfate (SO₄²⁻), and carbonate (CO₃²⁻) in simulated Hanford tank waste solutions containing NaOH were determined from oversaturation at 20 °C, 40 °C, 60 °C, and 80 °C after equilibration for 3 to 7 days by Barney (1976). The solubilities of the added salts were found to decrease in the order NaNO₂ > NaNO₃ >> Na₂CO₃ > Na₂SO₄ and decrease with increasing NaOH concentration. The salt solubilities [aside from NaAl(OH)₄] increased with temperature at higher NaOH concentrations. Concerns have been expressed that the 3- to 7-day equilibration times in the tests by Barney (1976) were inadequate to crystallize gibbsite from supersaturated solutions that also contained high concentrations of sodium salts (Reynolds and Reynolds 2010). The objections are based on the 4-week equilibration times observed by Herting et al. (1986) for simpler and less concentrated solutions at 80 °C and the high likelihood of ion pairing and [Al(OH)₄]⁻ dimerization in the concentrated liquors, both of which would inhibit nucleation and crystal growth. Observations qualitatively similar to those of Reynolds and Reynolds (2010) exist in the aluminum industry's Bayer process, in which oxyanions inhibit gibbsite precipitation (Hudson et al. 2012). As demonstrated in the Hanford-related technical literature and in the present tests, the nitrate and nitrite oxyanions both promote gibbsite dissolution and inhibit gibbsite precipitation. An additional comparison with Hanford tank waste solutions is provided in Appendix D (Figure D.2). The aluminum versus free hydroxide molar concentrations for tank waste solutions analyzed and reported in the TWINS database, as gathered by Agnew and Johnston (2013), are presented along with the gibbsite solubility values, in the same units, from the present testing at ~27 °C, 45 °C, and 80 °C. It can be seen that, although the presence of NaNO₃ and NaNO₂ goes some way to explaining the enhanced aluminum solubility in tank waste, there is still a significant gap between the values obtained in these tests, and the measured values for aluminum solubility in tanks. Clearly, there are additional solution components that have an effect on aluminum solubility. For example, the relatively high total organic carbon content measured in tank waste suggests the presence of organics, e.g. glycolate and oxalate (Kupfer et al., 1999), that act as nucleation inhibitors and help to stabilize NaAl(OH)₄ in solution, reducing the driving force for gibbsite precipitation. These additional solution components, in conjunction with NaNO₃ and NaNO₂, require further investigation.

3.2.7 Gibbsite Solubility in NaOH-NaAl(OH)₄-NaNO₂ Solutions

NaNO₂ without NaNO₃ was added to the NaOH-NaAl(OH)₄ solutions in tests T1, T5, and T9 at 27 °C, 45 °C, and 80 °C from undersaturation, respectively, and in test T13 at 45 °C from oversaturation. The final NaNO₂ concentrations ranged from 6.2 to 10.6 M and the final NaOH concentrations ranged from 0.45 to 1.2 M. The time required to reach equilibrium was within days, but final sampling for analysis occurred at the end of testing, from 84 to 143 days. The results for undersaturation presented here show that NaNO₂ enhances gibbsite solubility as compared to the concentrations predicted by the Misra Equation at the same hydroxide concentrations and temperatures by factors ranging from about 2 at 27 °C (T1; 6.3 M

NaNO₂) and 45 °C (T5; ~7.5 M NaNO₂) to 3.3 at 80 °C (T9; ~10 M NaNO₂). Comparing T5 and T9, at 45 °C and 80 °C, which have similar added NaNO₂ concentrations (7.5 and 10 M, respectively), it is seen that increasing temperature strongly enhances the impact of added nitrite. Furthermore, compared with NaNO₃ and the mixed NaNO₃/NaNO₂ tests, NaNO₂ has the largest positive effect on gibbsite solubility, under most test solution conditions. At 45 °C, the positive effect for nitrite is slightly greater for the test from oversaturation [T9; a solubility enhancement of a factor of three over the expected Misra Equation value in the nitrite-free system] compared with the similar test from undersaturation [T5; a factor of two greater than expected for the nitrite-free system] but it is likely that the oversaturation test concentration would converge to the undersaturation value in time.

There are no studies in the literature on the NaOH-NaAl(OH)₄-NaNO₂ system in the absence of other salts for comparison. More generally, however, in review of prior studies, Misra (1970) reported that both Na₂CO₃, and sodium chloride, NaCl, enhanced gibbsite solubility compared with the solubility found at otherwise similar conditions but in the absence of these salts. The relative solubility enhancement was about 15% at 60 °C and 95 °C for Na₂CO₃ and 20% for NaCl at 60 °C.

3.3 Solid Phase Characterization after Dissolution Tests

To determine the effect of solution conditions on the solid gibbsite phase, XRD patterns and SEM images were collected on the solids after the tests were completed for comparison with Figure 1 and Figure 2, respectively.

3.3.1 Effect of Dissolution from Undersaturation on Gibbsite Mineralogy and Particle Size

XRD on the solids for the tests at 27 °C, 45 °C, and 80 °C (Figure 16) confirms that gibbsite is the only crystalline mineral phase present and that no transformation to boehmite is observed, even after extended periods of dissolution at 80 °C. The peak widths (FWHM) observed in XRD patterns were significantly narrower when compared with those for the starting material (Figure 1), indicating an increase in the crystallite size. A similar increase in crystallite and particle size has been previously observed for gibbsite during dissolution in NaOH (3 M) at 80 °C (Graham et al. 2018). Additional solid phase characterization data are provided in Appendix E.

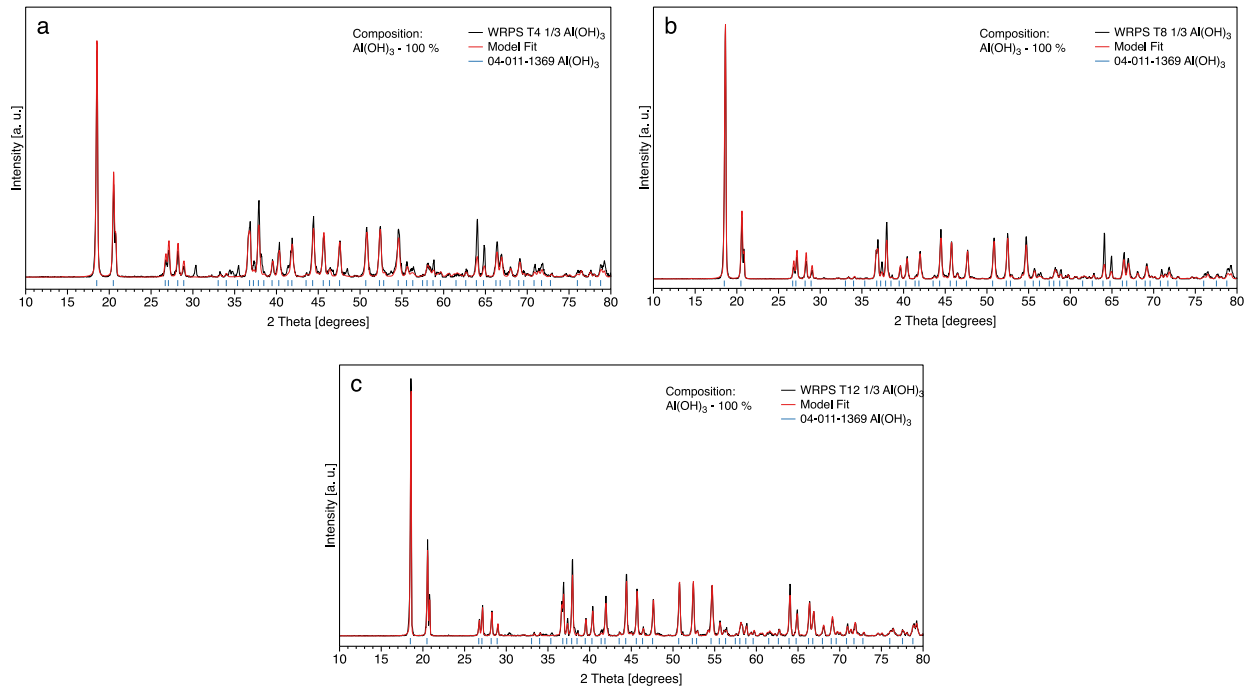


Figure 16. XRD showing changes to the gibbsite mineralogy and particle size at (a) 27 ± 2 °C (T4), (b) 45 ± 2 °C (T8), and (c) 80 ± 2 °C (T12) after exposure to NaOH solution

3.3.2 Effect of Dissolution from Undersaturation and Oversaturation on Gibbsite at 45 ± 2 °C

SEM and XRD were completed on the solid phases from all tests at 45 °C. SEM images of powders obtained from T5, T6, T7, and T8 experiments (Figure 17) show retention of the original pseudo-hexagonal plate-like morphology. Certain aspects of these particles, such as considerable rounding of the edges, is expected during a dissolution-precipitation process. Generally, gibbsite particles appear to be larger than the starting material, and in some instances (Figure 17d) new particle faces (i.e., 1 0 0, 1 1 0, and 0 1 1) are noted.

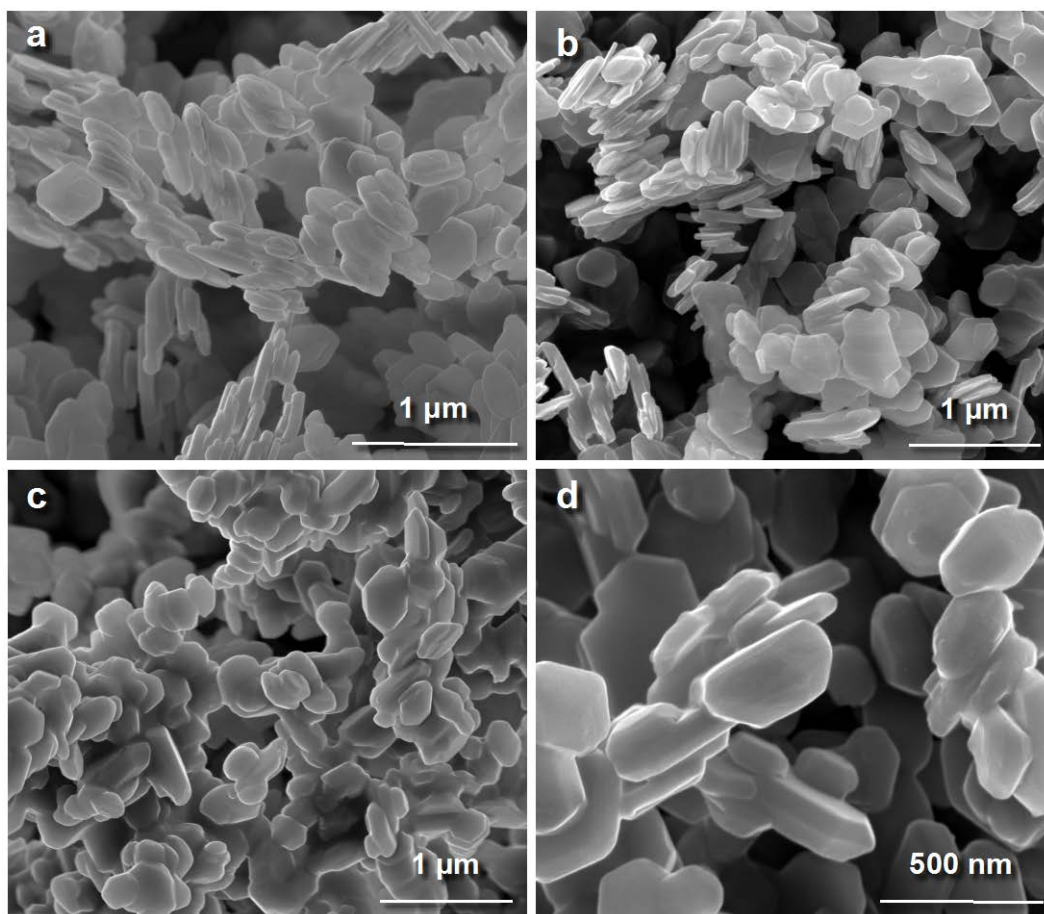


Figure 17. SEM Showing Changes to the Size and Morphology of Gibbsite Solid Phase at 45 ± 2 °C after Exposure to: (a) NaOH/NaNO₂ Solution (T5); (b) NaOH/NaNO₃ Solution (T6); (c) NaOH/NaNO₃/NaNO₂ Solution (T7); and (d) NaOH Solution (T8)

The XRD patterns for the solid gibbsite samples after dissolution at 45 °C (Figure 18) show that gibbsite is the only crystalline Al-bearing phase after dissolution, with small amounts of sodium nitrite and/or sodium nitrate (T6, T7). The peak widths (FWHM) observed in XRD patterns were significantly narrower when compared with those for the starting material (Figure 1), indicating an increase in the crystallite size in the z-axis (azimuthal direction) from $ca. 24 \pm 1$ nm to $ca. 42 \pm 1$, 43 ± 2 , 62 ± 2 , and 65 ± 2 nm for T5, T6, T7, and T8, respectively. A similar increase in crystallite and particle size has been previously observed for gibbsite during dissolution in NaOH (3 M) at 80 °C (Graham et al. 2018).

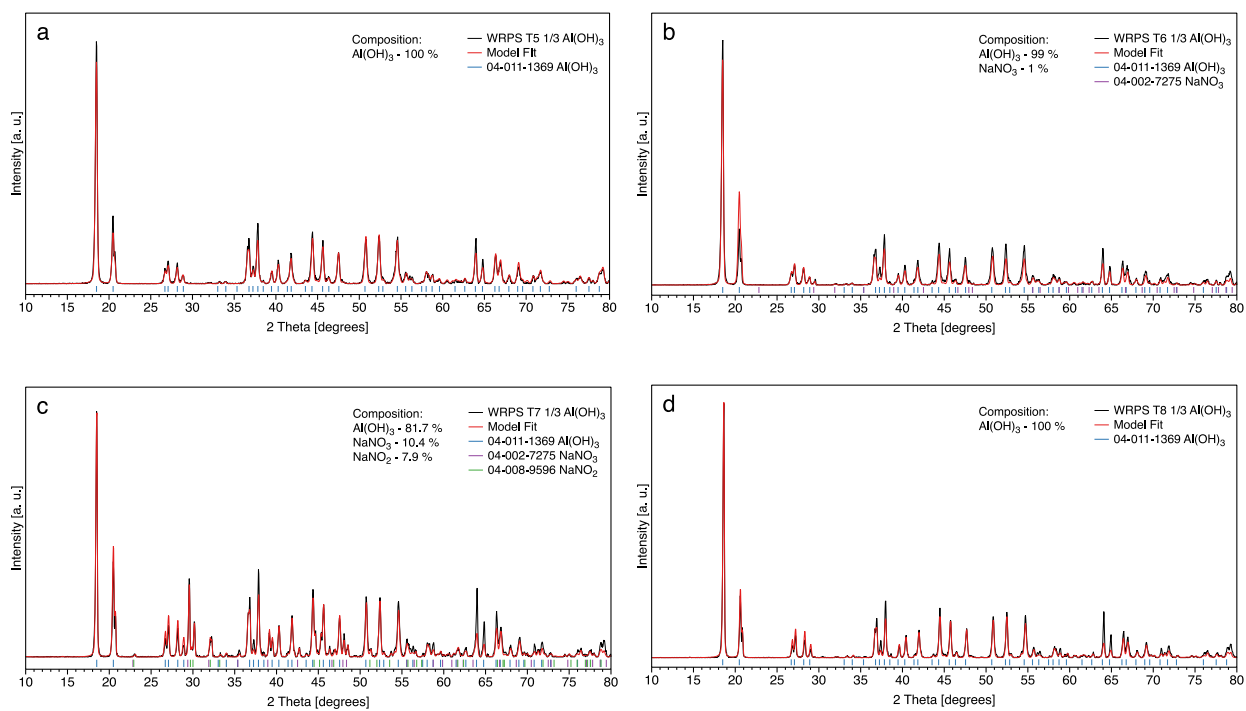


Figure 18. XRD Showing Changes to the Gibbsite Solid Phase and Crystallinity at $45 \pm 2^\circ\text{C}$ after Exposure to: (a) NaOH/NaNO₂ Solution (T5); (b) NaOH/NaNO₃ Solution (T6); (c) NaOH/NaNO₃/NaNO₂ Solution (T7); and (d) NaOH Solution (T8)

4.0 Summary and Conclusions

To establish a defensible technical basis for minimizing or avoiding aluminum hydroxide precipitation during DFLAW staged feed dilution, aluminum solubility must be predicted as a function of the significant variables that influence gibbsite dissolution and precipitation. The variables investigated in the present testing include (1) temperature (27 °C, 45 °C, and 80 °C); (2) equilibration time (up to 143 days); (3) NaNO₃, NaNO₂, and NaOH (individually and in combination) that are present in high concentrations in the Hanford tank waste at levels that may significantly affect the activity coefficient of either hydroxide or the aluminate ion; (4) the presence and absence of gibbsite seed crystals; and (5) the approach from above and below saturation. Seventeen data points for gibbsite solubility in solutions containing NaOH, NaNO₂, and NaNO₃ were obtained for a range of solution conditions at different temperatures over a period of up to 143 days.

The four tests conducted for the simple NaOH-NaAl(OH)₄ system showed gibbsite solubilities in general agreement with the solubilities projected by the prediction equation established by Misra (1970). This prediction equation, based on measurements compiled from the technical literature, includes data from 25 to 100 °C and total caustic concentrations of ~1 to 7.4 M as sodium hydroxide and aluminate and thus encompasses the conditions of the present testing. As noted in Section 3.2.3, however, the data used to inform the Misra model at the higher temperatures and higher total alkalinities generally lie below the values predicted by the Misra Equation [see Figures 1(a) and 1(b) of Misra 1970]. Thus, the differences noted between the gibbsite solubilities observed for test T12 and the Misra (1970) model prediction are reasonable.

The presence of added NaNO₃, NaNO₂, and NaNO₃-NaNO₂ in combination enhanced the aluminum solution concentration (gibbsite solubility) above that expected from the Misra Equation at the same respective NaOH concentrations but in the absence of added salt. The solubility enhancements observed at 27 °C for NaNO₃ and NaNO₂ were a factor of 1.6 and 2.2, respectively; those at 45 °C were a factor of 1.4 and 2.5, respectively, with nitrite showing a greater effect than nitrate most likely because it was at a higher concentration. The solubility enhancement at 80 °C for NaNO₂ was a factor of 3.3, while that for NaNO₃ was a factor of 2.5 compared with the solubility expected by the Misra Equation in the absence of added nitrite or nitrate.

The tests from oversaturation, for the NaOH-NaAl(OH)₄ system as well as for the other three systems containing added NaNO₃, NaNO₂, and both NaNO₃-NaNO₂, maintained, for up to seven weeks, consistently greater aluminum concentrations than their analogous tests conducted from undersaturation. It was only when gibbsite nanoplate seed crystals were added to the tests from oversaturation that the same equilibration aluminum solution concentrations were attained as those for tests from undersaturation.

Tabulated solute concentration data and solution densities from the solubility tests are provided in Appendix D as potential input to more sophisticated chemical models. Also provided in Appendix D is a comparison of the data from this report with aluminum versus free hydroxide molar concentrations for tank waste solutions, demonstrating that there is still a gap between the aluminum solubility in NaNO₃/NaNO₂-containing solutions and the aluminum solubility in the tank waste. Additional investigation of aluminum solubility in other components of the tank waste solution is required to fully explain this enhanced solubility.

Characterization of the beginning and final solid phases also was performed. The initial gibbsite particles (nanoplates) had diameter and average thickness of 332 ± 73 nm and 29 ± 7 nm, respectively, and showed only gibbsite to be present by XRD. The XRD pattern showed some line broadening, indicating the small

crystallite size. The solid phase remained gibbsite, as shown by XRD, after each test but the line sharpness increased, indicating recrystallization occurred to form larger crystallites. The SEM images showed an increase in the azimuthal (z-axis) dimension of the plates so that they became more equant in aspect. The particles also agglomerated, as would be expected from the recrystallization that would occur by gibbsite aging in saturated solution.

4.1 Proposed Task 3 Work Scope

To establish a defensible technical basis for minimizing or avoiding aluminum hydroxide precipitation during DFLAW staged feed dilution, aluminum solubility must be predicted as a function of the significant variables that influence gibbsite dissolution and precipitation. One significant variable is the concentration of sodium nitrite in solution as a function of temperature, as this affects the activity coefficient of the hydroxide and the aluminate ion. There are very few studies of the NaNO_2 - NaOH - H_2O system in the literature. Plekhotkin and Bobrovskaya (1970) measured the solubility of NaNO_2 in NaOH solutions at 20 °C and obtained the 25 °C solubility isotherm; however, no data above room temperature are available. Reynolds and Herting (1984) describe the NaNO_2 solubility limit in NaOH solutions at a range of temperatures, but the solutions also contain ethylenediaminetetraacetic acid (EDTA), tetrasodium salt, trisodium citrate, sodium phosphate, sodium carbonate, and sodium sulfate. The proposed task will close the identified data gap associated with the NaNO_2 - NaOH - H_2O system at temperatures greater than 25 °C.

The experiments will build on those described in this report, and expand the knowledge of sodium nitrite solubility in a NaOH solution as provided by Plekhotkin and Bobrovskaya (1970) and Reynolds and Herting (1984) so that essential thermodynamic parameters for sodium nitrite may be obtained to model the more complex Hanford tank waste solutions. Key experimental conditions and limits are listed below.

- Concentrated stock solutions of NaOH will be prepared and stored in a glovebox under an argon atmosphere to minimize carbonate formation from atmospheric carbon dioxide.
- NaOH concentrations in the 0–6.0 m range (to cover range of solution conditions analyzed here) will be investigated.
- Anticipated NaNO_2 solubilities will be estimated from data for the solubility of NaNO_2 from Plekhotkin and Bobrovskaya (1970) and Washburn (1928), and a 30% excess of NaNO_2 will be added to the NaOH solutions at a given temperature.
- Experiments will be conducted at 27, 40, 60 and 80 °C [spanning the temperature in the tanks, up to the leaching temperature in the Hanford Tank Waste Treatment and Immobilization Plant (WTP)] with shaking in sealed Teflon containers.
- Aliquots will be collected, filtered at temperature, and immediately diluted with water.
- The mass of a known volume from each test solution will be recorded at temperature to determine the solution density.
- The diluted solutions will be analyzed by inductively coupled plasma-optical emission spectroscopy (ICP-OES) for Na, and ion chromatography (IC) for nitrite; free hydroxide will be determined by titration.
- The analytical work will be performed in the ESL, which operates under a QA program that implements HASQARD and NQA-1.
- Tests will be allowed to equilibrate for one week at temperature prior to sampling for nitrite solubility.

The proposed experimental work outlined above, representing Task 3 work scope for FMP-DFLAW-25, will be planned, executed, and formally reported as a data package.

4.2 Recommendations for Follow-On Work

The work proposed here will close many identified gaps in predicting aluminum hydroxide solubility with dilution and temperature. The experiments will encompass effects of temperature, equilibration time, and specific solution components. However, the integrated flowsheet model and tank farm operations would further benefit from conducting additional experiments to accomplish the following:

- Understand the effect of gibbsite particle size and mass loading on the solution chemistry and aluminum hydroxide solubility.
- Include Na_2CO_3 in the solution composition matrix to determine its effect on $\text{NaAlCO}_3(\text{OH})_2$ dissolution and precipitation in the presence of $\text{Al}(\text{OH})_3$.
- Although not a laboratory study, systematically survey the TWINS data to identify the impacts of tank waste components on the dissolved aluminum concentration in solution as functions of free hydroxide concentration and temperature. Do this by comparing these TWINS aluminum concentration data with the concentrations expected by way of the Misra Equation at the same temperature for the simple $\text{NaOH-NaAl}(\text{OH})_4$ system.
- Identify the specific tank waste components most responsible for increasing or decreasing the equilibrium aluminum concentration by conducting gibbsite solubility tests at a single selected temperature and NaOH molality in the presence and absence of the selected tank waste components. The selected components would include the major inorganic species (e.g., sodium salts of nitrate, nitrite, carbonate, sulfate, phosphate, fluoride, chloride) and organic species known to be present in the tank waste (e.g., sodium salts of EDTA, HEDTA, formate, glycolate, citrate, gluconate, and oxalate).
- Understand the effect of seed crystals at different temperatures so that diluted tank waste solutions can potentially be seeded with $\text{Al}(\text{OH})_3$ to induce precipitation and mitigate the effects of unanticipated solids carryover into the LAWPS, delayed aluminum precipitation fouling the LAWPS ion exchange operations, and transfer line deposition.
- Extend the timescale of the experiments to encompass kinetic effects on $\text{Al}(\text{OH})_3$ precipitation over periods relevant to diluted DFLAW storage (i.e., one to nine months).
- Define key counterion (Na^+) concentrations to stabilize polymeric aluminum solution species and limit precipitation.
- Identify the presence of polymeric aluminum solution species and/or $\text{NO}_2^- - \text{Al}(\text{OH})_4^-$ complexes using Raman spectroscopy and ^{27}Al nuclear magnetic resonance (NMR) spectroscopy and determine their role in stabilizing supersaturated Al solutions.

Ultimately, this additional work would provide key information about (1) the mechanisms by which gibbsite becomes supersaturated; (2) $\text{Al}(\text{OH})_3$ precipitation kinetics, including induction times to precipitation; and (3) potential blending strategies to minimize $\text{Al}(\text{OH})_3$ precipitation.

This program of work is timely because it would leverage PNNL's current IDREAM EFRC and multi-million dollar investments in nuclear process science to develop a predictive understanding of concentrated alkaline aluminum-containing solutions of relevance to DFLAW.

5.0 References

- Agnew SF and CT Johnston. 2013. *Aluminum Solubility in Complex Electrolytes*. Paper 13011 at WM2013 Conference, February 24-28, 2013, Phoenix, Arizona. <http://www.wmsym.org/archives/2013/papers/13011.pdf>.
- Anderson KA, MD Britton, JM Colby, LH Cree, MS Fountain, DW Nelson, VC Nguyen, and ME Stone. 2017. *One System River Protection Project Integrated Flowsheet*. RPP-RPT-57991, Rev. 3, 24590-WTP-RPT-MGT-14-023, Rev. 2, Washington River Protection Solutions LLC, Richland, Washington.
- Barney GS. 1976. *Vapor-Liquid-Solid Phase Equilibria of Radioactive Sodium Salt Wastes at Hanford*. ARH-ST-133, Atlantic Richfield Hanford Company, Richland, Washington.
- Bénézech P, S Hilic, and DA Palmer. 2016. "The Solubilities of Gibbsite and Bayerite Below 100 °C in Near Neutral to Basic Solutions." *Journal of Solution Chemistry* 45:1288-1302.
- Delegard CH, CI Pearce, and MS Fountain. 2018. *Precipitation Risk when Diluting DFLAW Feed Saturated in Aluminum Hydroxide*. PNNL-27312, RPT-OSIF-002, Rev. 0, Pacific Northwest National Laboratory, Richland, Washington.
- Felmy AR, JR Rustad, MJ Mason, and R de la Bretonne. 1994. *A Chemical Model for the Major Electrolyte Components of the Hanford Waste Tanks: The Binary Electrolytes in the System: Na-NO₃-NO₂-SO₄-CO₃-F-PO₄-OH-Al(OH)₃-H₂O*. PNL-SA-23952, Pacific Northwest Laboratory, Richland, Washington.
- Graham TR, M Dembowski, E Martinez-Baez, X Zhang, NR Jaegers, J Hu, MS Gruskiewicz, H-W Wang, AG Stack, ME Bowden, CH Delegard, GK Schenter, AE Clark, SB Clark, AR Felmy, KM Rosso, and CI Pearce. 2018. "In-Situ ²⁷Al NMR Spectroscopy of Aluminate in Sodium Hydroxide Solutions Above and Below Saturation with Respect to Gibbsite" *Inorganic Chemistry*. Accepted.
- Herting DL. 2014. *Effect of Phosphate, Fluoride, and Nitrate on Gibbsite Dissolution Rate and Solubility*. LAB-RPT-13-00011, Rev. 0, Washington River Protection Solutions, LLC, Richland, Washington. <http://www.iaea.org/inis/collection/NCLCollectionStore/Public/45/068/45068209.pdf>
- Herting DL, GA Cooke, JS Page, and JL Valerio. 2015. *Hanford Tank Waste Particle Atlas*. LAB-RPT-15-00005 R0, Washington River Protection Solutions LLC, Richland, Washington.
- Herting D, T Welsh, and D Reynolds. 1986. *Gibbsite Equilibrium in Simulated Liquid Waste*. RHO-SD-WM-TI-211, Rev. 0, Rockwell Hanford Operations. Richland, Washington.
- Hudson LK, C Misra, AJ Perrotta, K Wefers, and FS Williams. 2012. "Aluminum Oxide." From *Ullmann's Encyclopedia of Industrial Chemistry*. Wiley-VCH Verlag GmbH & Co. KGaA, Weinheim, Germany.
- Kupfer MJ, AL Boldt, KM Hodgson, LW Shelton, BC Simpson, RA Watrous, MD LeClair, GL Borsheim, RT Winward, BA Higley, RM Orme, NG Colton, SL Lambert, and DE Place. 1999. *Standard Inventories of Chemicals and Radionuclides in Hanford Site Tank Wastes*. HNF-SD-WM-TI-740, Rev. 0C, Lockheed Martin Hanford Company, Richland, Washington

McCoskey JK, GA Cooke, and DL Herting. 2015. *Chemical Equilibrium of Aluminate in Hanford Tank Waste Originating from Tanks 241-AN-105 and 241-AP-108*. LAB-RPT-14-00011 R0. Washington River Protection Solutions LLC, Richland, Washington.

Misra C. 1970. "Solubility of aluminium trihydroxide (hydrargillite) in sodium hydroxide solutions." *Chemistry and Industry* 19(5):619-623.

NQA-1-2000, *Quality Assurance Requirements for Nuclear Facility Applications*. American Society of Mechanical Engineers, New York, New York.

NQA-1-2008, *Quality Assurance Requirements for Nuclear Facility Applications*. American Society of Mechanical Engineers, New York, New York.

NQA-1a-2009, *Addenda to ASME NQA-1-2008*. American Society of Mechanical Engineers, New York, New York.

Orme RM. 2003. *Hanford Tank Waste Operations Simulator Specific Gravity Model – Derivation of Coefficients and Validation*. RPP-14767, Rev. 0, Hanford Numatec Corporation. Richland, Washington.

Plekhotkin, VF and LP Bobrovskaya. 1970. "The $\text{NaNO}_2\text{-NaOH-H}_2\text{O}$ and $\text{NaNO}_3\text{-NaOH-H}_2\text{O}$ Systems". *Russian Journal of Inorganic Chemistry* 15:842-844.

Reynolds DA and DL Herting. 1984. *Solubilities of Sodium Nitrate, Sodium Nitrite, and Sodium Aluminate in Simulated Nuclear Waste*. RHO-RE-ST-14P, Rockwell Hanford Operations, Richland, Washington.

Reynolds JG and DA Reynolds. 2010. *A Modern Interpretation of the Barney Diagram for Aluminum Solubility in Tank Waste*. Paper 10075 at WM2010 Conference, March 7-11, 2010, Phoenix, Arizona.

Reynolds JG, JK McCoskey, and DL Herting. 2016. "Gibbsite Solubility in Hanford Nuclear Waste Approached from above and below Saturation." *Industrial & Engineering Chemistry Research* 55:5465-5473. <http://dx.doi.org/10.1021/acs.iecr.6b00743>.

Reynolds JG, DR Reinemann, MS Fountain, ME Stone, and RB Wyrwas. 2017. *One System River Protection Project Integrated Flowsheet Maturation Plan*. RPP-PLAN-58003, Rev. 3, 24590-WTP-PL-MGT-15-0011, Rev. 2, Washington River Protection Solutions LLC, Richland, Washington.

Russell RL, HD Smith, DE Rinehart, and RA Peterson. 2009. *Development and Characterization of Gibbsite Component Simulant*. PNNL-18013, WTP-RPT-176, Rev. 0, Pacific Northwest National Laboratory, Richland, Washington.

Washburn EW. 1928. International Critical Tables of Numerical Data, Physics, Chemistry and Technology, Vol. III and IV. McGraw-Hill Book Company, Inc., New York, New York.

Zhang X, X Zhang, TR Graham, CI Pearce, BL Mehdi, AT N'Diaye, S Kerisit, ND Browning, SB Clark, and KM Rosso. 2017. "Fast Synthesis of Gibbsite Nanoplates and Process Optimization using Box-Behnken Experimental Design." *Crystal Growth & Design*, 17:6801-6808

Appendix A

Experimental Set-Up Pictures

Appendix A

Experimental Set-Up Pictures



Figure A.1. Experimental Set-Up for 27 °C Tests



Figure A.2. Experimental Set-Up for 45 °C and 80 °C Tests

Appendix B

Starting Solution Conditions for Sodium Hydroxide Containing Sodium Nitrite/Nitrate

Appendix B

Starting Solution Conditions for Sodium Hydroxide Containing Sodium Nitrite/Nitrate

Table B.1. Make-Up and Measured Concentrations for Nitrate and Nitrite

Test Number	Make-up Concentration						Measured Starting Conc. (IC), M		Rel. % Difference, IC vs Make-up	
	Molality, m			Molarity, M *						
	NaOH	NaNO ₃	NaNO ₂	NaOH	NaNO ₃	NaNO ₂	NaNO ₃	NaNO ₂	NaNO ₃	NaNO ₂
T0	1.01	0.00	0.00	1.01	0.00	0.00	-	-	-	-
T1	1.03	0.00	7.05	0.86	0.00	5.89	-	6.00	-	1.9
T2	1.03	4.91	0.00	0.89	4.23	0.00	4.10	-	-3.1	-
T3	1.02	5.46	4.98	0.77	4.15	3.79	3.95	3.78	-4.7	-0.1
T4	6.07	0.00	0.00	6.03	0.00	0.00	-	-	-	-
T5	1.02	0.00	8.49	0.82	0.00	6.87	-	7.06	-	2.9
T6	1.04	6.34	0.00	0.86	5.25	0.00	5.18	-	-1.4	-
T7	4.03	5.07	5.02	3.08	3.88	3.85	3.52	3.96	-9.4	2.8
T8	6.11	0.00	0.00	6.06	0.00	0.00	-	-	-	-
T9	2.00	0.00	9.99	1.57	0.00	7.82	-	8.11	-	3.7
T10	1.98	7.97	0.00	1.57	6.32	0.00	6.13	-	-3.0	-
T11	2.05	6.49	9.89	1.38	4.38	6.67	4.02	6.63	-8.2	-0.5
T12	6.15	0.00	0.00	6.11	0.00	0.00	-	-	-	-
T13	1.01	0.00	8.85	0.81	0.00	7.10	-	7.17	-	1.0
T14	1.00	6.15	0.00	0.83	5.12	0.00	5.13	-	0.1	-
T15	4.03	5.20	5.09	3.07	3.96	3.88	3.45	3.80	-13.0	-1.9
T16	6.09	0.00	0.00	6.04	0.00	0.00	-	-	-	-
								Average	-5.3	1.2
								Standard Deviation	4.4	1.9

* Molarity calculation based on solution density estimate through equation by Orme (2003)

Appendix C

Gibbsite Solubility Tests at 80 °C

Appendix C

Gibbsite Solubility Tests at 80 °C

Visual examination of the aluminum concentration versus time plots (Figure 3 through Figure 6; see also Table 3) shows that tests at 80 °C (Figure 5 and Figure 6) have greater variability than those at a lower temperature. In addition, the later samples in the 80 °C tests have greater variability than those with less contact time. To determine if consistent trends could be discerned, the aluminum concentrations logged as functions of time for the individual triplicate tests were assessed. The results of the assessment are presented here.

It was found that, like the averaged aluminum concentration values from the triplicate runs, the individual triplicate experiments at 80 °C showed increasing variability in aluminum concentration for each test condition as contact time increased. The results were plotted for each of the 80 °C tests (T9 through T12) to illustrate these trends (Figure C.1–Figure C.4, respectively). The starting solution compositions in each test, based on actual masses of material added, are shown in Table C.1, with concentrations provided in molality (m) and molarity (M). Also shown are the average aluminum concentrations calculated for periods judged to be at steady state or equilibrium and the standard deviations and RSDs of the aluminum concentrations. These averages and standard deviations included all of the concentration data (i.e., including all of the triplicate tests) for the selected steady concentration intervals.

Table C.1. Experimental Conditions and Findings for Tests Run at 80 °C

Test	Temp., °C	[NaOH]		[NaNO ₃]		[NaNO ₂]		Average [Al], M	Std. Dev. [Al], M	Rel. Std. Dev., %
		m	M	m	M	m	M			
T9	80	2.00	1.57	0.00	0.00	9.99	7.82	0.916	0.144	16
T10	80	1.98	1.57	7.97	6.32	0.00	0.00	0.787	0.176	22
T11	80	2.05	1.38	6.49	4.38	9.89	6.67	0.827	0.077	9
T12	80	6.15	6.11	0.00	0.00	0.00	0.00	2.262	0.276	12

As seen in Figure C.1 through Figure C.3 for tests T9, T10, and T11, all with ~2 m NaOH initially, aluminum concentrations increased with time until steady concentrations were reached at about 27 days of contact. For tests T10 and T11, relatively steady aluminum concentrations were maintained until about 83 days although for test T10 (Figure C.2), an appreciable aluminum concentration dip occurred in all three of the triplicates at the 56-day measurement, likely due in part to a temporary decrease in temperature of the hot plate to 73.7 °C in the area of the T10 tests at the time of sampling. For the majority of the tests conducted at 80 °C, an increase from the steady concentration occurred in the subsequent measurements at 83 and 91 days. This is due to a loss in integrity of the reaction vessel seals at these longer test times, leading to evaporation.

Steady aluminum concentrations were reached in shorter times for test T12 run using the more concentrated 6 m NaOH initial solution. Figure C.4 shows that steady aluminum concentrations were reached by 6 days of contact and maintained through 42 days. After that, a dip in the aluminum concentration occurred in all three of the triplicates at the 56-day measurement. The concentration swings up in the measurements at 83 and 91 days due to evaporation. This identical pattern is seen for tests T10 and T12 at the same sampling times of 56, 83, and 91 days because the T10 and T12 tests were located in the same area of the heating block and subject to the same temperature drop at 56 days.

Overall, the concentration alterations at the longer contact times for these 80 °C tests followed a consistent upward trend, as would be expected if water were lost from the solutions due to evaporation, increasing the residual NaOH concentration and favoring gibbsite dissolution. Thus, the final values for solubility provided in Table D.1 represent a more concentrated system than the reported equilibrium values (Table C.1). However, as shown in Figure 3, even at 27 °C, due to the small particle size and high surface area of the gibbsite nanoplates, equilibrium is reached very rapidly (within one day), so the aluminum concentrations do represent the equilibrium values for the test conditions in Table D.1, in terms of hydroxide as determined by acid titration, and nitrate/nitrite as determined by IC analysis.

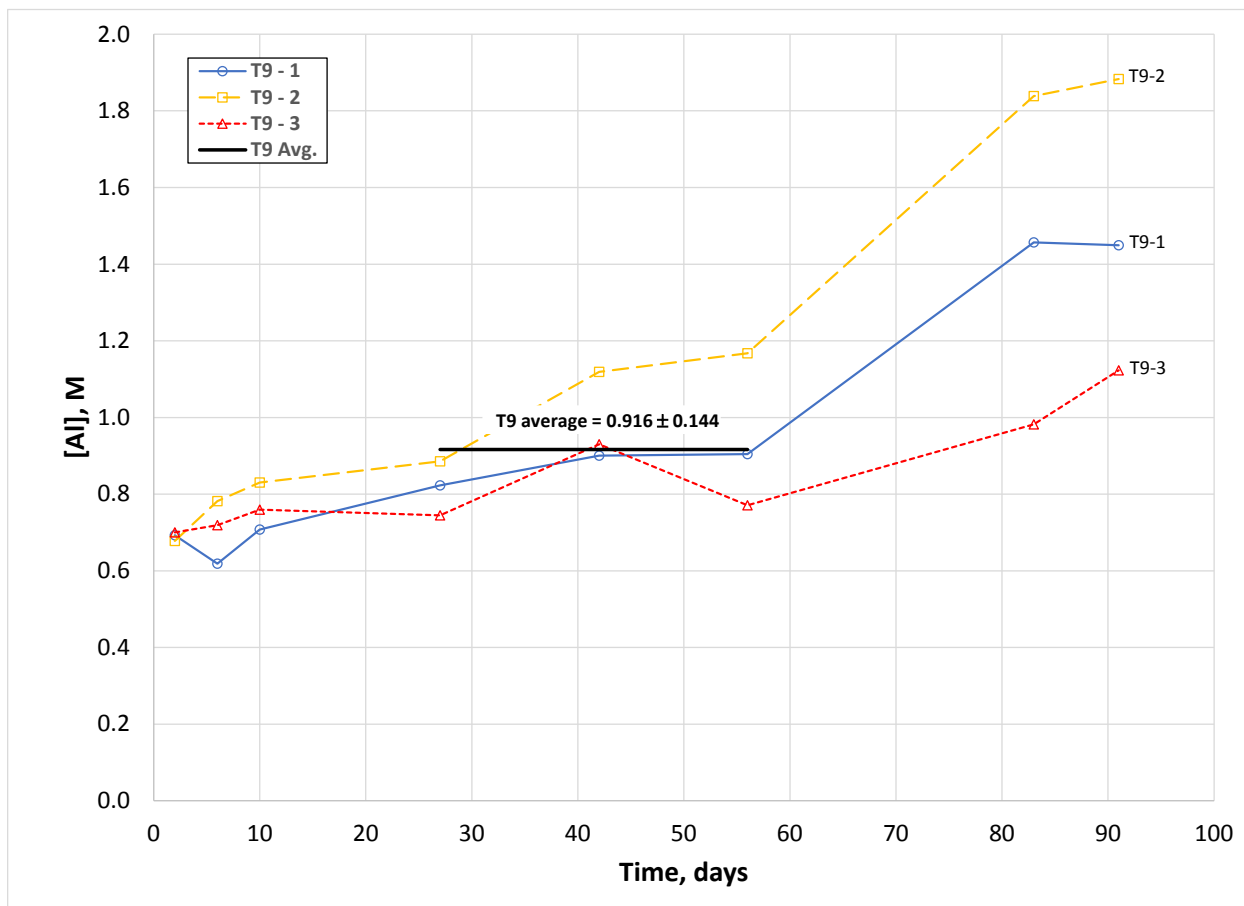


Figure C.1. Gibbsite Solubility in 2 m NaOH/10 m NaNO₂ at 80 °C (Test T9)

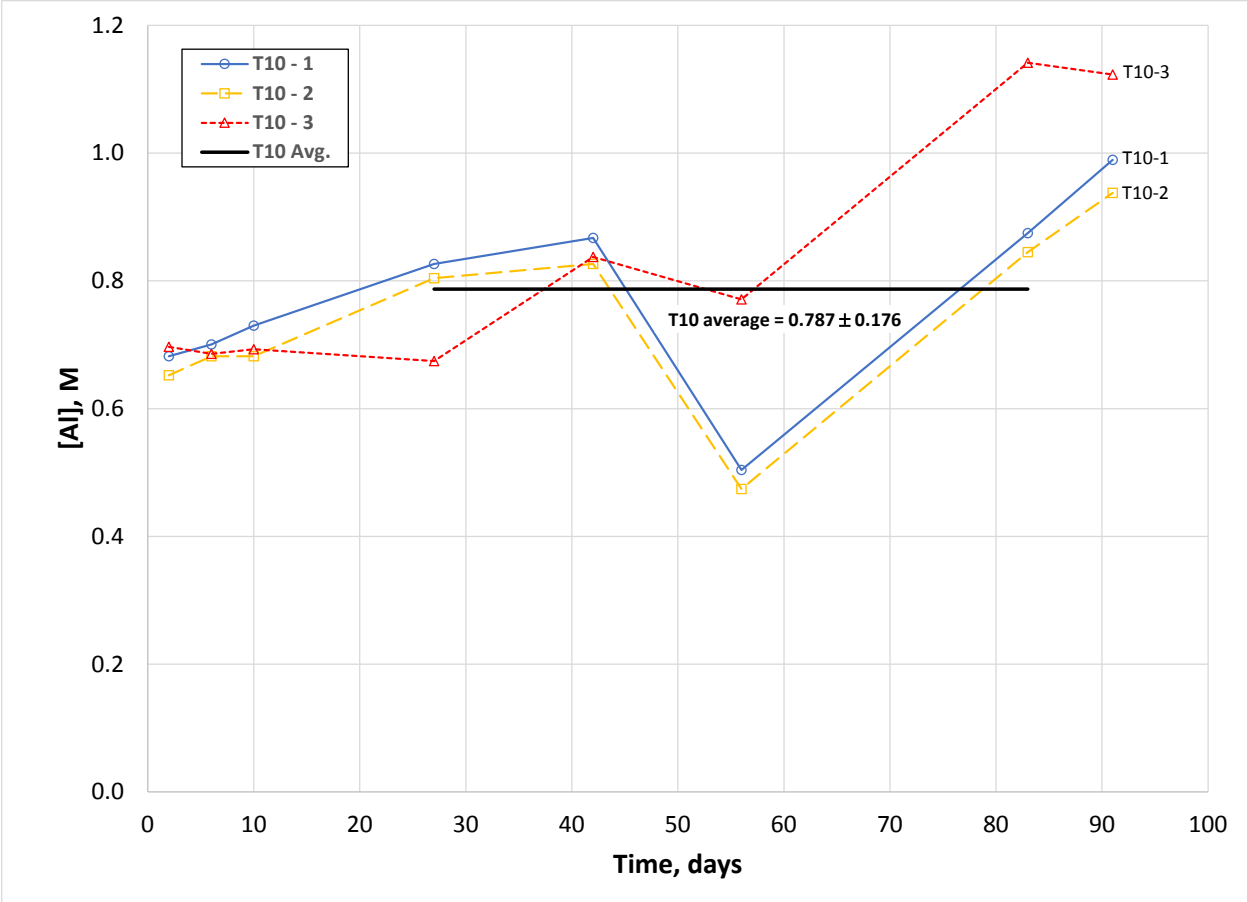


Figure C.2. Gibbsite Solubility in 2 m NaOH/8 m NaNO₃ at 80 °C (Test T10)

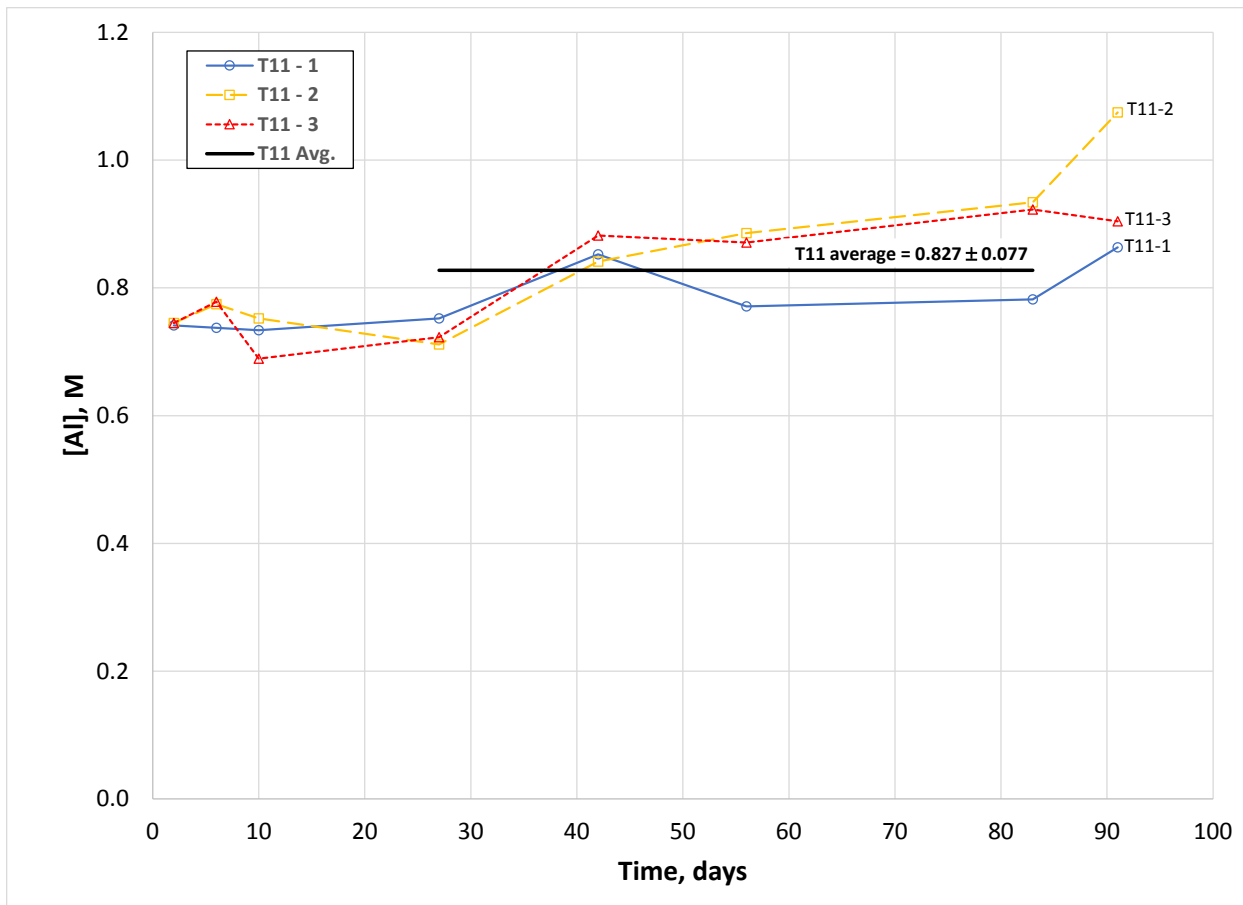


Figure C.3. Gibbsite Solubility in 2 m NaOH/6.5 m NaNO₃/10 m NaNO₂ at 80 °C (Test T11)

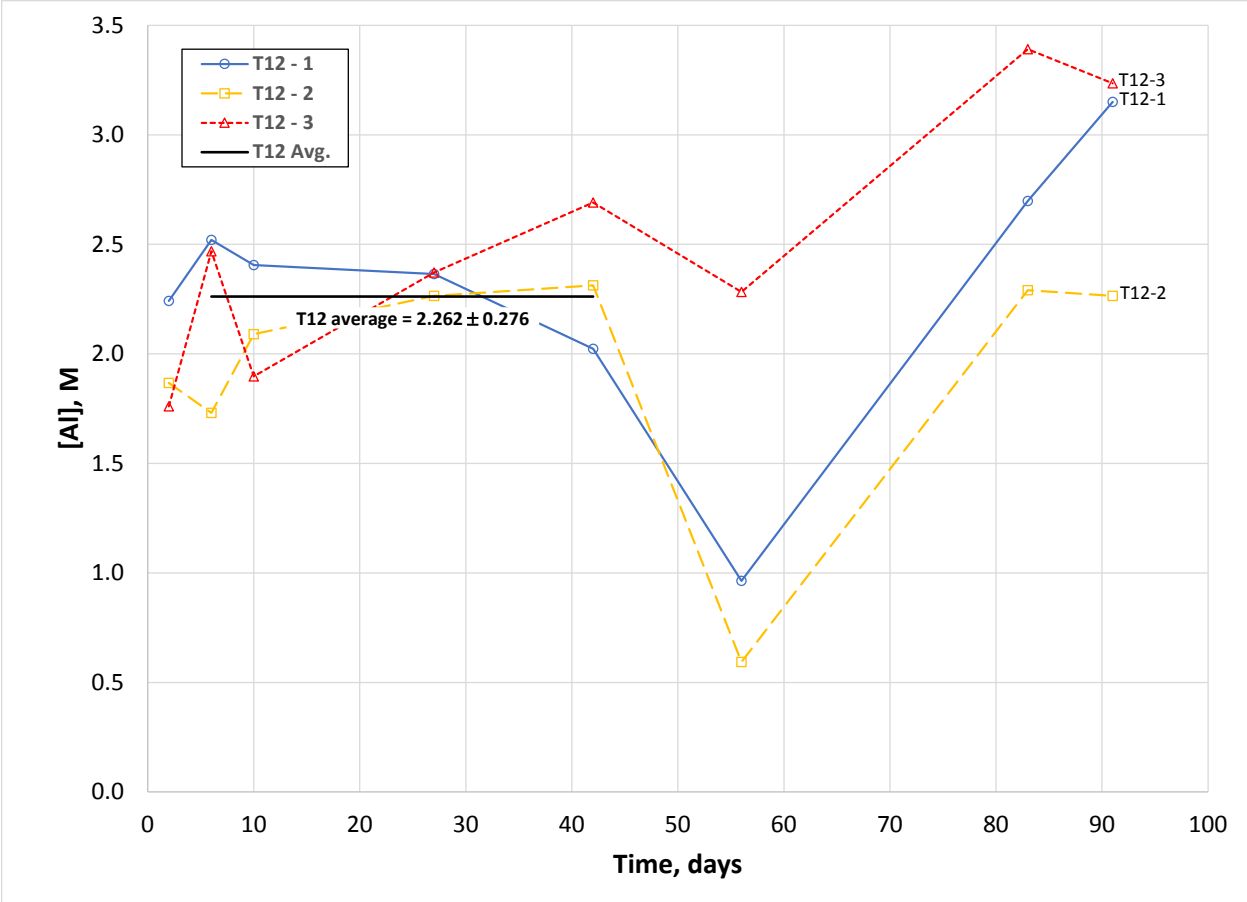


Figure C.4. Gibbsite Solubility in 6 m NaOH at 80 °C (Test T12)

Appendix D

Gibbsite Solubility Data

Appendix D

Gibbsite Solubility Data

The sensitivity of gibbsite solubility to the test temperature (provided gibbsite solid phase is present) is demonstrated by the aluminum concentration response of tests T1 through T3 as the experimental temperature varied from 24.1 to 28.6 °C. All of the aluminum concentration data, from samplings done from 3 to 146 days, are plotted in Figure D.1. Though scatter is observed, the slopes of the aluminum concentrations versus temperature plots for the tests T1, T2, and T3 are remarkably consistent, rising about 0.0043 molar per degree. This rise is somewhat steeper than that obtained using the Misra Equation, for “pure” (salt-free) NaOH/NaAl(OH)₄ solutions at about 0.0023 molar per degree.

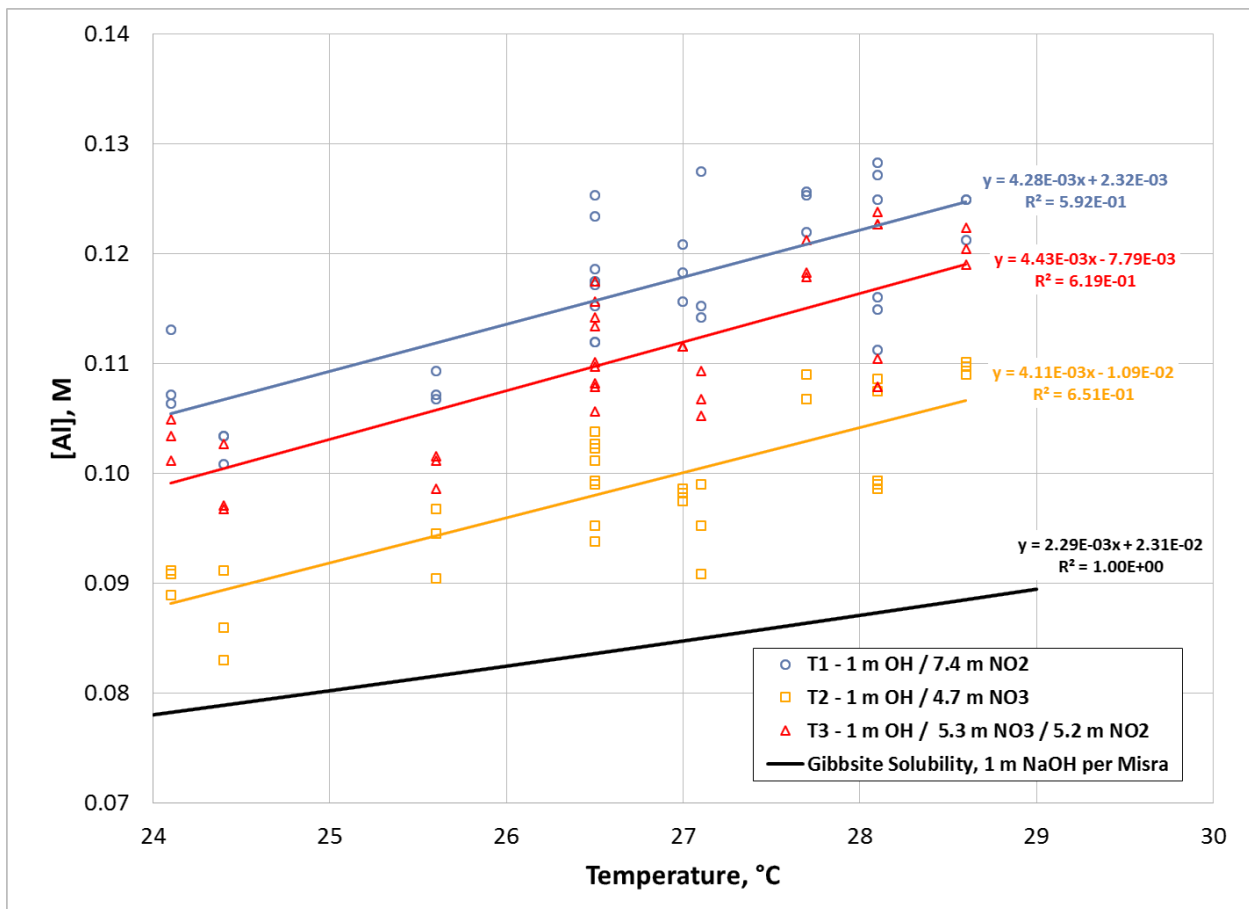


Figure D.1. Dependence of Gibbsite Solubility on Temperature in Tests T1, T2, and T3

The data for the test solutions at the final samplings are shown in Table D.1 and include each of the triplicates. Thus, three sets of values are provided for tests T0 through T16, all performed in triplicate.

These data include the measured values for test temperature, solution density at that temperature, and molar solution concentrations for total alkalinity (titration to pH 8.3, thus including hydroxide plus aluminate), as well as aluminum as measured by ICP, and nitrate and nitrite by IC. The net molar concentration of “free” hydroxide was calculated as the difference between the total alkalinity and the

aluminum concentration. The solution concentrations also are converted to units of molality by calculation based on the measured molar concentrations and measured densities.

Figure D.2 shows aluminum versus free hydroxide molar concentrations for tank waste solutions analyzed and reported in the TWINS database as gathered by Agnew and Johnston (2013). Also presented in Figure D.2 are the gibbsite solubility values, in the same units, from the present testing at ~27 °C, 45 °C, and 80 °C. It is seen that the 27 °C data for the current tests are clearly below the $[\text{OH}^-]/[\text{Al}] = 1.5$ and 2.0 thresholds, the 45 °C near the $[\text{OH}^-]/[\text{Al}] = 2.0$ line (except for the data for both temperatures from the 6 m NaOH tests having no added NaNO_3 or NaNO_2 whose data points are clustered above ~4 M OH^-), and the 80 °C data above the $[\text{OH}^-]/[\text{Al}] = 1.5$ line (except for the data for the 6 m NaOH tests, which are between the two lines). Overall, the 27 °C and 45 °C solubilities are in the realm of the actual tank waste data, except for the 6 m tests findings for which no tank waste data at such high OH^- concentrations are found. The 80 °C solubilities likely do not correspond with the tank waste data because of the higher (and uncharacteristic) temperature compared with actual tank waste storage conditions. Given that some of the $[\text{Al}]$ values for the tank waste solutions are still much higher than those in $\text{NaNO}_3/\text{NaNO}_2$ -solutions tested here, there are additional components of the tank waste solutions that play a role in stabilizing $\text{NaAl}(\text{OH})_4$ in solution.

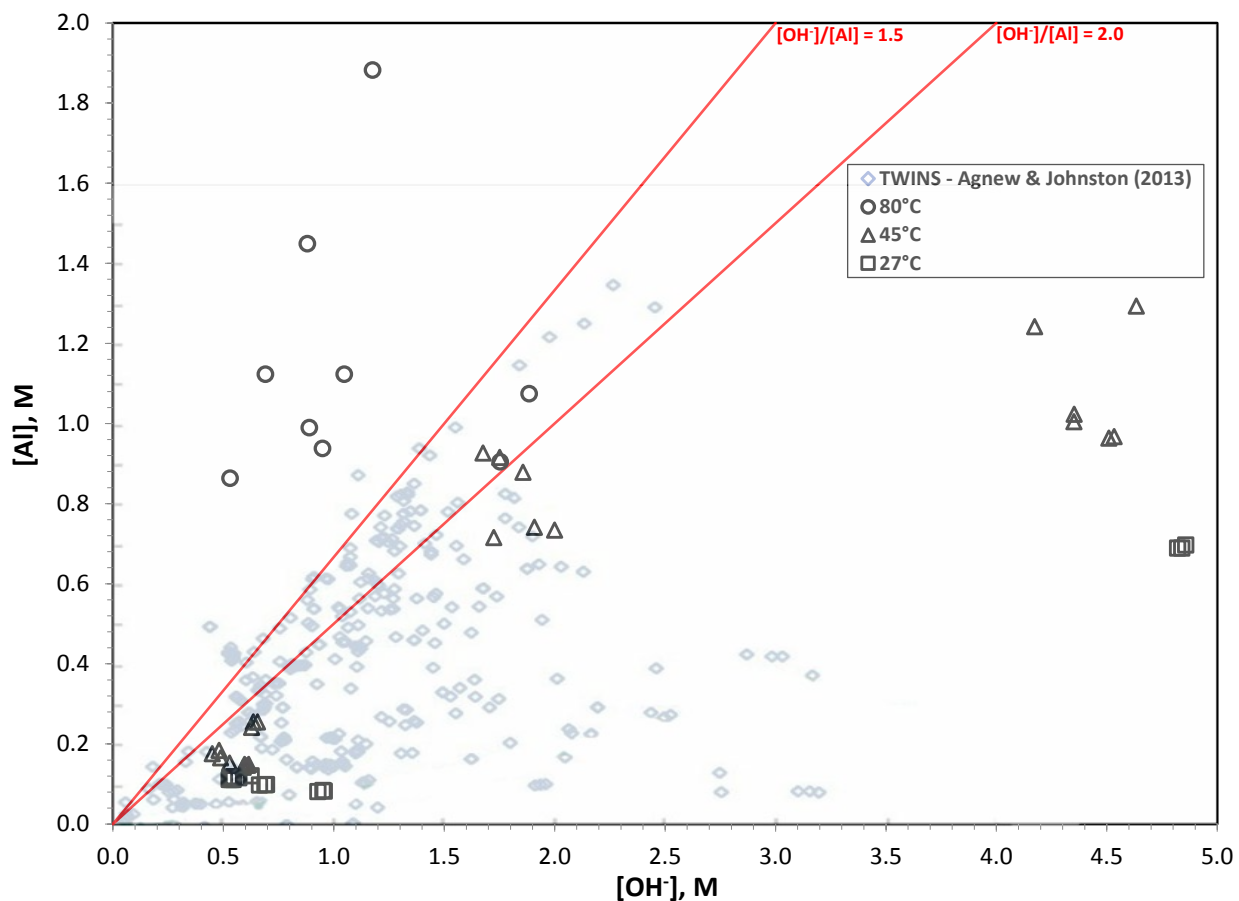


Figure D.2. FOR INFORMATION ONLY. Comparison of Current Test Solubilities with Solution Analyses for Undisturbed, REDOX Sludge and S-Saltcake, and Aluminum Cladding Removal Wastes from TWINS and TWINS Values for Tank Wastes at 3 to 7 M Total Sodium (taken from Figure 1 of Agnew and Johnston 2013)

Table D.1. Test Solution Temperatures, Densities, and Solute Concentrations at the Final Samplings

Test	Rep.	Temp., °C	Dens., g/cm ³	[Alk] _{tot.} , M	[OH] _{free} , M	[Al], M	[NO ₃ ⁻], M	[NO ₂ ⁻], M	(OH) _{free} , m	(Al), m	(NO ₃ ⁻), m	(NO ₂ ⁻), m
T0	1	27.1	1.087	1.035	0.951	0.084	0.00	0.00	0.915	0.081	0.00	0.00
	2	27.1	1.080	1.009	0.928	0.082	0.00	0.00	0.898	0.079	0.00	0.00
	3	27.1	1.083	1.040	0.957	0.083	0.00	0.00	0.925	0.080	0.00	0.00
T1	1	27.0	1.312	0.663	0.545	0.118	0.00	6.24	0.644	0.140	0.00	7.38
	2	27.0	1.322	0.685	0.570	0.116	0.00	6.33	0.671	0.136	0.00	7.45
	3	27.0	1.310	0.746	0.626	0.121	0.00	6.26	0.746	0.144	0.00	7.46
T2	1	27.0	1.295	0.794	0.695	0.099	4.23	0.00	0.775	0.110	4.71	0.00
	2	27.0	1.295	0.786	0.688	0.098	4.14	0.00	0.762	0.109	4.59	0.00
	3	27.0	1.294	0.761	0.663	0.097	4.21	0.00	0.739	0.109	4.69	0.00
T3	1	27.0	1.418	0.656	0.544	0.112	4.02	3.96	0.708	0.145	5.22	5.15
	2	27.0	1.412	0.637	0.526	0.112	4.03	3.96	0.690	0.146	5.29	5.19
	3	27.0	1.414	0.646	0.535	0.112	4.02	3.98	0.700	0.146	5.26	5.21
T4	1	27.0	1.277	5.510	4.820	0.689	0.00	0.00	4.806	0.687	0.00	0.00
	2	27.0	1.272	5.529	4.839	0.689	0.00	0.00	4.854	0.691	0.00	0.00
	3	27.0	1.277	5.554	4.857	0.697	0.00	0.00	4.855	0.696	0.00	0.00
T5	1	43.3	1.325	0.626	0.450	0.176	0.00	7.54	0.587	0.230	0.00	9.85
	2	43.3	1.319	0.653	0.487	0.166	0.00	7.54	0.642	0.218	0.00	9.93
	3	43.3	1.333	0.665	0.480	0.184	0.00	7.69	0.631	0.242	0.00	10.11
T6	1	43.3	1.325	0.680	0.528	0.152	5.32	0.00	0.633	0.183	6.38	0.00
	2	43.3	1.322	0.745	0.596	0.149	5.40	0.00	0.726	0.181	6.58	0.00
	3	43.3	1.301	0.764	0.615	0.149	5.08	0.00	0.743	0.180	6.14	0.00
T7	1	43.3	1.432	2.649	1.908	0.741	3.44	3.54	2.607	1.013	4.69	4.84
	2	43.3	1.466	2.733	2.000	0.734	3.44	3.56	2.626	0.964	4.51	4.68
	3	43.3	1.454	2.439	1.724	0.715	3.39	3.48	2.231	0.926	4.38	4.50
T8	1	43.3	1.238	5.356	4.351	1.004	0.00	0.00	4.602	1.062	0.00	0.00
	2	43.3	1.255	5.500	4.533	0.967	0.00	0.00	4.724	1.008	0.00	0.00
	3	43.3	1.250	5.375	4.352	1.023	0.00	0.00	4.556	1.071	0.00	0.00
T9	1	80.4	1.483	2.329	0.880	1.449	0.00	10.43	1.579	2.602	0.00	18.73
	2	80.4	1.436	3.058	1.175	1.883	0.00	9.59	2.325	3.725	0.00	18.96
	3	80.4	1.459	1.813	0.690	1.123	0.00	10.59	1.214	1.975	0.00	18.62
T10	1	80.4	1.471	1.878	0.889	0.990	8.03	0.00	1.397	1.556	12.63	0.00
	2	80.4	1.485	1.886	0.948	0.938	8.24	0.00	1.491	1.474	12.96	0.00
	3	80.4	1.505	2.170	1.047	1.123	9.56	0.00	2.023	2.169	18.47	0.00
T11	1	80.4	1.576	1.394	0.530	0.864	4.84	8.09	1.097	1.785	10.00	16.71
	2	80.4	1.600	1.656	0.581	1.075	5.47	7.76	1.291	2.389	12.15	17.25
	3	80.4	1.575	1.415	0.510	0.904	4.81	8.02	1.050	1.861	9.89	16.50
T12	1	80.4	1.323	7.305	4.155	3.150	0.00	0.00	5.292	4.013	0.00	0.00
	2	80.4	1.321	6.337	4.073	2.264	0.00	0.00	4.572	2.542	0.00	0.00
	3	80.4	1.418	7.641	4.406	3.235	0.00	0.00	5.123	3.762	0.00	0.00
T13	1	46.8	1.368	0.891	0.635	0.255	0.00	8.96	0.915	0.368	0.00	12.89
	2	46.8	1.360	0.869	0.627	0.242	0.00	8.93	0.909	0.350	0.00	12.95
	3	46.8	1.376	0.910	0.655	0.255	0.00	9.13	0.949	0.370	0.00	13.23
T14	1	45.2	1.314	0.746	0.599	0.147	4.73	0.00	0.687	0.169	5.42	0.00
	2	45.2	1.312	0.756	0.609	0.147	4.90	0.00	0.714	0.172	5.74	0.00
	3	45.2	1.308	0.732	0.590	0.142	4.89	0.00	0.692	0.167	5.73	0.00
T15	1	45.2	1.461	2.735	1.856	0.878	3.56	3.78	2.581	1.221	4.96	5.26
	2	45.2	1.458	2.666	1.751	0.915	3.52	3.74	2.421	1.266	4.86	5.17
	3	45.2	1.469	2.602	1.675	0.927	3.58	3.78	2.303	1.274	4.92	5.20
T16	1	46.8	1.261	5.927	4.633	1.293	0.00	0.00	5.019	1.401	0.00	0.00
	2	46.8	1.236	5.414	4.173	1.242	0.00	0.00	4.523	1.346	0.00	0.00
	3	46.8	1.246	5.473	4.510	0.964	0.00	0.00	4.737	1.012	0.00	0.00

* T0 total alkalinity determined by sodium (ICP). All other total alkalinity determined by acid titration to pH 8.3

Appendix E
Post-Test XRD

Appendix E

Post-Test XRD Data

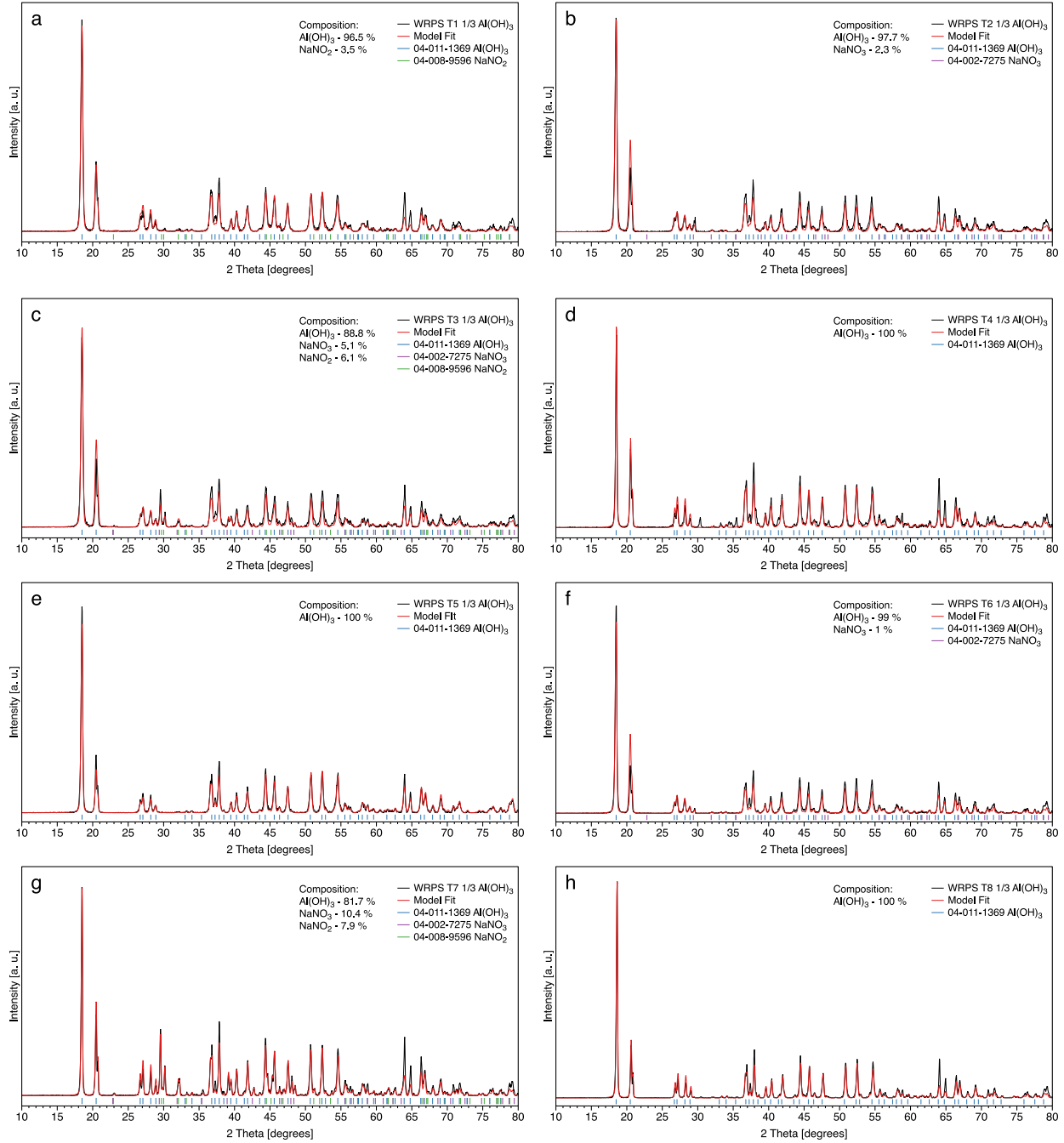


Figure E.1. XRD Showing Changes to the Gibbsite Solid Phase and Crystallinity for Tests T1 – T8 (a-h)

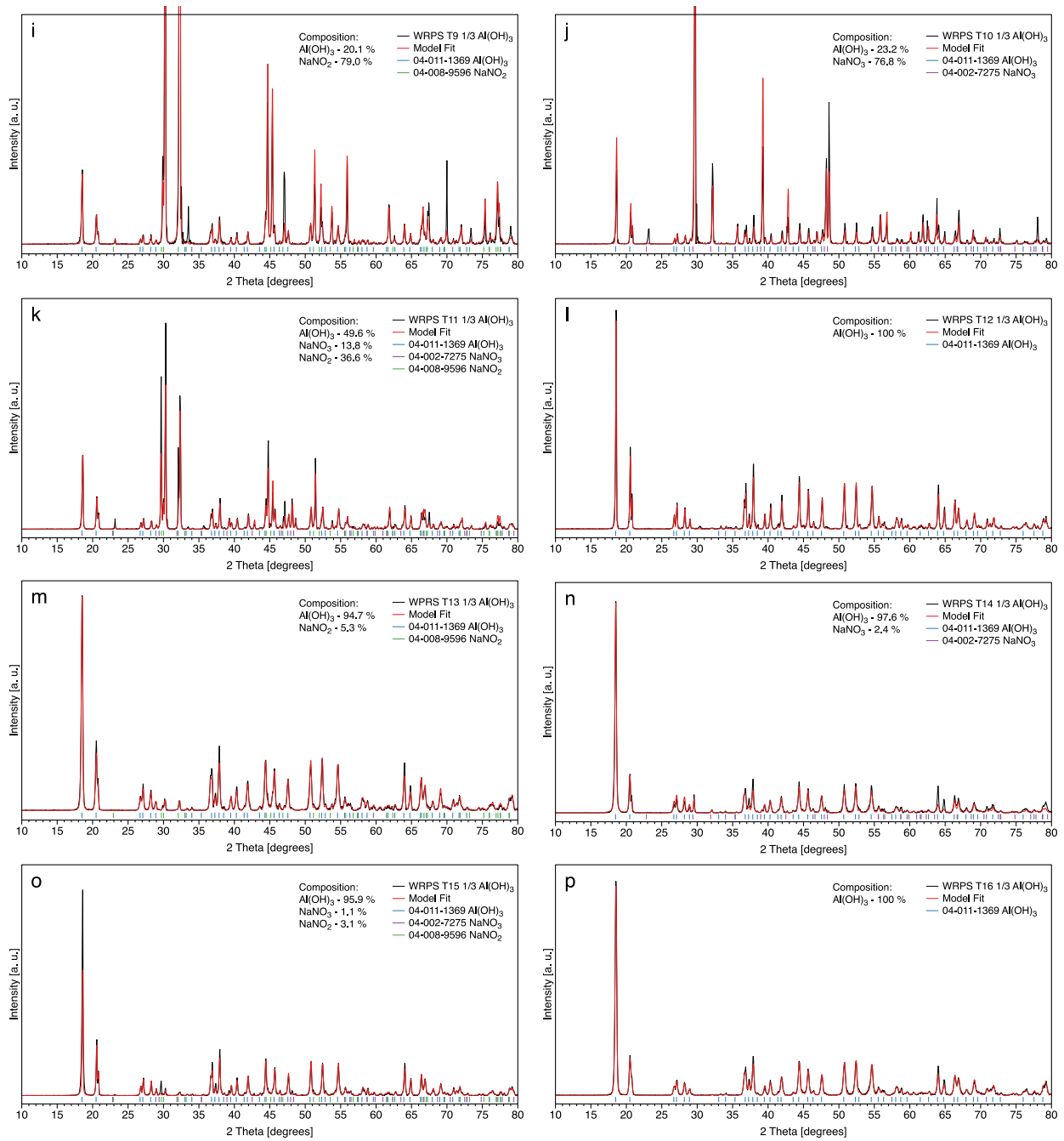


Figure E.2. XRD Showing Changes to the Gibbsite Solid Phase and Crystallinity for Tests T9–T16 (i-p)

Distribution

All distributions of the current report will be made electronically. PDF copies may also be available from the PNNL-publications website (<http://www.pnnl.gov/main/publications>).

TradeWind Services, LLC
CH Delegard

Washington River Protection Solutions LLC
MD Britton
JG Reynolds

Pacific Northwest National Laboratory
SR Baum
CLH Bottenus
M Dembowski
MS Fountain
II Leavy
RA Peterson
MMV Snyder
Information Release
Project File



**Pacific
Northwest**
NATIONAL LABORATORY

www.pnnl.gov

902 Battelle Boulevard
P.O. Box 999
Richland, WA 99352
1-888-375-PNNL (7665)

U.S. DEPARTMENT OF
ENERGY